# Characterization of boron-doped single-crystal diamond by electrophysical methods (review)

© V.I. Zubkov,[1] A.V. Solomnikova,[1] A.V. Solomonov,[1] A.V. Koliadin,[2] J.E. Butler[1,3]

[1] St. Petersburg State Electrotechnical University „LETI" St. Petersburg, Russia
[2] OOO NPK Almaz, Sestroretsk, Russia
[3] Cubic Carbon Ceramics, MD Huntingtown, USA
e-mail: solomnikova-anna@yandex.ru

A critical analysis of the existing methods of controlling the concentration of impurity and majority charge carriers in wide bandgap semiconductors and the issues of improvement of modern diagnostics of the main electrophysical properties of single-crystal diamond are considered based on the results of our studies and the works of other authors. It was found that independent assessment of impurity concentration and concentration of free charge carriers is of fundamental importance for semiconductor diamond due to very low (less than 1%) degree of ionization of the introduced impurity. The advantages and prospects of admittance spectroscopy as a diagnostic method for ultrawide bandgap semiconductors are shown and solutions aimed at the correct interpretation of the experimental data are proposed. The high ionization energy of boron impurity in diamond (370 meV) results in a strong frequency dispersion of the measured barrier capacitance. It is shown that under disturbance of quasi-static conditions in capacitance-voltage measurements, low frequencies and high temperatures should be used for correct assessment of the charge carrier concentration. The results of electrophysical studies are compared with traditional measurements of impurity concentration in diamond by optical methods. A decrease of hole activation energy from the boron impurity level from 325 to 100 meV was found upon increasing the boron concentration NA from $2 \cdot 10^{16}$ to $4 \cdot 10^{19}$ cm$^{-3}$. The transition to the hopping mechanism of conductivity within the impurity (acceptor) band with thermal activation energy of $10-20$ meV was registered for $N_A \geq 5 \cdot 10^{18}$ cm$^{-3}$ at temperatures of $120-150$ K.

**Keywords:** single-crystal diamond, boron impurity, charge carrier concentration, activation energy, admittance spectroscopy, capacitance-voltage measurements.

## Introduction

The unique electrophysical and mechanical properties of diamond make it possible to consider it as a quite promising material for being used in power and optical electronics as well as operated in extreme conditions [1–6]. For the high-voltage electronics, the diamond-based semiconductor devices can significantly reduce energy consumption and increase limit breakdown voltages, an operating frequency and temperature [7–11]. Low coefficients of adhesion and friction in diamond (as compared to silicon) demonstrate advantages of application of diamond films in micro-electromechanical (MEM) devices [12–15].Undoped diamond can be used to create sensors of charged particles, X-ray and ultraviolet radiation [16–18], as well as to create UV photodetectors [19,20]. On the other hand, impurity doping to the ultra-high level in extremely narrow layers (δ-doping) is considered as a real way of creating powerful unipolar transistors [21–25].

The present review consists of two parts. The first part is dedicated to critical analysis of the existing methods of synthesis and doping of the single-crystal diamond as well as to controlling the concentration of impurities and majority charge carriers (MCC) in wide bandgap semiconductors as well as to improving diagnostics of the main electrophysical properties of the boron-doped single-crystal diamond. The key diagnostics method used in the present work is admittance spectroscopy. It is a non-destructive method, which can be used to carry out quantitative measurements of static and dynamic characteristics of the charge carriers and impurity centers in order to predict properties of manufactured instrument structures.

The second part, which is an experimental one, is dedicated to careful determination of the concentration of the majority charge carriers (holes) and the boron activation energy in diamond samples using temperature and frequency admittance spectroscopy methods in conditions of substantially incomplete ionization, which are inherent to this semiconductor. The results obtained are compared with measurement results obtained by other authors. It proposes solutions aimed at correct interpretation of the experimental data.
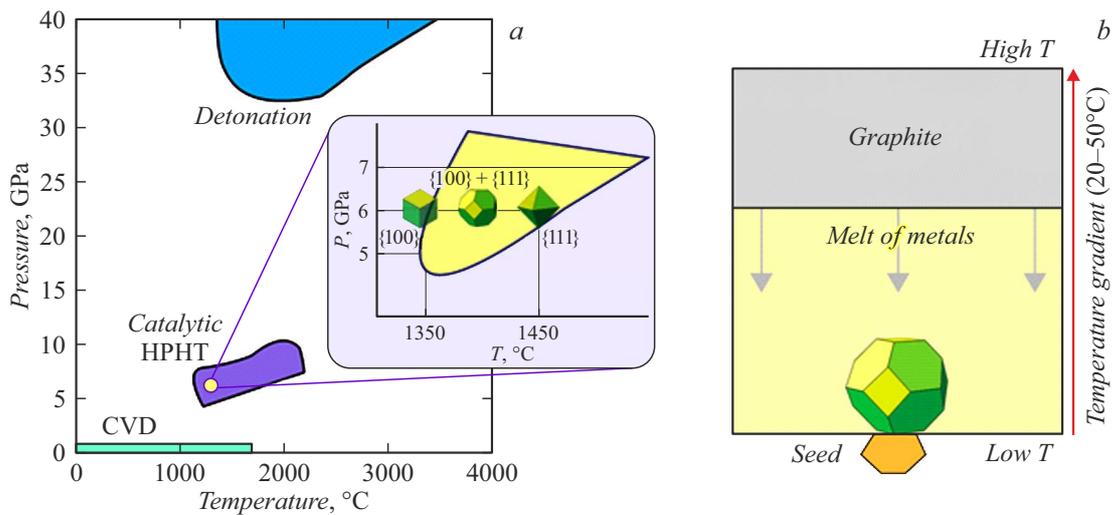
**Figure 1.** *a* — the phase diagram with growth conditions of the single-crystal diamond in the HPHT and CVD methods; *b* — the scheme of diamond growing in the HPHT method.

## 1. Theoretical analysis

### 1.1. Methods of synthesis and doping of single-crystal diamond

The last decade has witnessed a serious progress in a technology of synthesis of diamonds of highly structural perfection [26]. Now we can say that the two main crystal growth methods — the HPHT method (high pressure high temperature) and the CVD method (chemical vapor deposition) are approximately at the same technological level, whereas each of them has its own features and growth conditions (Fig. 1, *a*).

The bulk diamond crystals are successfully grown by the HPHT method at the temperatures of $1400 \pm 50°$C and the pressures of about $5-6$ GPa; while modern growth plants of the Cubic type can provide for high hydrostatic pressure by means of six ultra-high pressure cylinders [27–29]. As represented by the „New Diamond Technology" (NDT), Russia is a world leader in this field [30,31]. Thus, — in 2020 the company reported about synthesized single crystals of the weight of more than 100 carats. The HPHT diamond growth fundamentally differs from the planar growth of common semiconductors using the Czochralski method, the band melting method, etc. in simultaneous growth of crystal faces out of the bulk seeding all at once at several directions (Fig. 1, *b*). It is obvious that during the crystal HPHT growth the first appearing faces are defined by orientation of the crystal seeding and are perpendicular to the main growth direction. Further on, in the conditions of free growth of many faces all at once the crystal habitus is formed by a ratio of their growth rates, which primarily depend on the growth temperature provided that the press pressure is unchanged. When the temperature varies within the said ranged, it can result in producing the bulk crystals of the cubic, cuboctahedral, rhombohedral and other forms.

The morphology of the growing crystal can be conveniently described by the parameters $\alpha_v$, which are defined by the ratio of the face growth rates, for example, $\alpha_v = \sqrt{3}v_{001}/v_{11}$ for the faces (001) and (111), respectively [32]. In accordance with the Curie-Wulff principle underlaying the molecular-kinetic theory of crystal growth, a crystal surface will have the most developed faces with the lowest growth rates [33]. As a result, the forming crystal is governed by the dominating growth of simply formed faces with the biggest interplanar distance {100}, {110}, {111}, {113}.

The cuboctahedral diamond shape is the most preferred one for practical microelectronical applications. It is implemented with the ratio of the growth rates for the [001] and [111] directions $v_{001}/v_{111} \approx 1.15$ [34], which corresponds to $\alpha_v \sim 2$.

The HPHT-synthesized crystal is cut to parallel-plane plates for the subsequent post-growth technological operations. A set of the plates cut from one impurity-doped diamond crystal is shown on Fig. 2.

The epitaxial layers and the individual bulk diamond crystals are produced by chemical vapor deposition (CVD). For implementation of this method one should mention the works [35–41]. The CVD crystal growth requires a diamond single-crystal substrate, which is usually a HPHT-produced plate. The standard CVD-growth method is based on plasma activation of hydrogen atoms and carbon-containing radicals, whose subsequent deposition to the substrate ensures formation of the diamond film as a result of a complex of surface chemical reactions. For the effective growth of the diamond films it is necessary to provide for non-equilibrium concentration of atomic hydrogen near the substrate surface [42].

Modern commercial CVD reactors with the plasma activation can be used to grow the diamond epitaxial films with the rate above $1 \mu$m/h [43]. It is ensured
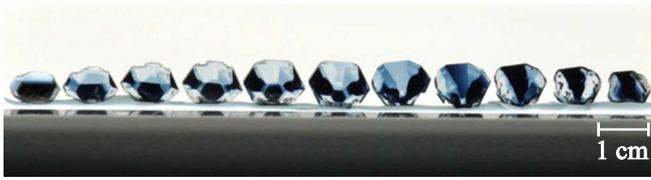
**Figure 2.** Set of the multi-sector diamond plates, which are cut from the HPHT crystal grown by NDT.

by effective diffusion transfer of the ionized particles and radicals ($CH_3$, $C_2H_2$, H) out of the plasma bulk to the substrate. The typical process of deposition of the diamond films with the plasma activation is realized at the pressure from 100 to 200 Torr (1 Torr $\approx$ 133.3 Pa) by magnetron UHF radiation of the frequency of 2.45 GHz. The substrate temperature is maintained within the range of $700-1100°C$ [44,45]. The films are doped during the growth by using ethanol-dissolved impurity sources, in particular, trimethyl borate $B(OCH_3)_3$ for incorporation of boron [46].

Note that along with the single-crystal diamond, detonation nano-diamonds have become widespread, which are synthesized by detonation of powerful explosives in a closed chamber [47]. These nano-diamonds are applied as a cross-linking agent by adding into concrete and other building materials. They are used for polishing processes, in galvanic production, medicine and biology [48–52].

The undoped, chemically pure diamond is a perfect dielectric. Its intrinsic charge carrier concentration is evaluated to be $10^{-27}$ cm$^{-3}$ at the room temperature. The microelectronical significance is provided to this material due to possible incorporation of a large concentration of a dopant. However, due to the high atomic density of the diamond, there are only a few chemical elements which can integrate into its crystal lattice and change the type of the electrical conductance, which is critical for their instrument applications. In practice, today the most important dopants include nitrogen, boron and phosphorus. During the growth, the diamond is doped in both the methods (HPHT and CVD). Beside the *in situ* doping, in some cases impurity implantation is used to create the doping profile in a near-surface region (for the depth of several $\mu$m). Sometimes, the irradiation by high-energy particles [53–55] and the implantation of various impurities are used to incorporate color centers, thereby modifying the crystal color for jewellery applications [56] or for subsequent application as ultraviolet and ionising radiation dosimeters [57].

The nitrogen atom in its isolated form (as a substitution impurity) as well as in a composition of all possible compounds (first of all, with vacancies) creates very deep levels in a diamond band gap (1.6 eV from the conduction band bottom and deeper [58,59]). In this regard, it is difficult to consider it as a potential dopant in terms of the traditional microelectronics. On the other hand, due

to the formation of the NV-centers (the nitrogen-carbon vacancy complex) the nitrogen-doped diamonds have a high potential of their use in the photonics as single-phase radiation sources, in quantum cryptography [60–64] as well as in studies within quantum calculations [65]. Note also that for these problems usability of other color centers in diamond is widely studied, too. SiV [66,67], MgV [68,69], SnV [70,71].

The boron-doped diamond crystals are now considered as a base for future new generation instruments of optical- and micro-electronics and investigated by scientific groups around the world [72–77]. The applications of the boron-doped semiconductor diamond include the power and extreme electronics, two-spectrum photodetectors (deep ultra-violet and near-IR) [78]), etc. In recent years, another application field is intensely developing - biosensorics, which is due to biocompatibility of diamond and its very wide electrochemical window [79,80], which is sized by changing the boron concentration. The exceptional chemical resistance of diamond also accounts for its use as an electrode material in electrochemistry [81,82].

The anisotropy of the growth rate of various faces of the diamond crystal is also accompanied by a different speed of incorporation of the impurity thereinto [83,84]. The concentration of the interstitial boron impurity turns out to be bigger in the crystal faces oriented in the directions [111] and [110] and lesser for the (100) surface. Based on measurement of the charge carrier concentration in the variously oriented planes of the diamond plate, in the work [84] we have determined a relative value of the capture coefficients $K$ of the boron impurity for the faces as $K(111) : K(110) : K(100) = 18 : 9 : 1$. The various speeds of incorporation of the impurity into substrates of the various crystal-lattice orientation are especially critical for delta-doping [85,86], when the concentration of the impurity being incorporated is high and the operation time is calculated in several seconds.

Thus, along with the high potential capabilities of diamond, there are some serious problems in its semiconductor application due to the anisotropy of the growth and doping of the single crystal, the wide band gap and the very small ionization degrees of the interstitial impurity. In this regard, it is a priority task to study and control the electric properties of the boron-doped diamond as a physical and technological base of the instruments of diamond optical- and micro-electronics. Accordingly, the role of precise and reliable diagnostics of the impurity composition of the synthesized diamond structures increases with toughening the requirements to the material itself.

## 1.2. Methods of measurement of the concentration of the impurity and the majority charge carriers in diamond. Comparative analysis

The key physical characteristics of any semiconductor instrument include the concentration and the mobility of

the charge carriers. As will be shown in the review hereinafter, for diamond, it turns out to be crucial to separately determine the concentration of the interstitial (boron) impurity and the concentration of the free charge carriers (holes) p achieved at the operating temperature of the instrument. It is due to an extremely low degree of thermal ionization of boron atoms (fractions of a percent at the room temperature).

The widespread methods of controlling the impurity concentration and the mobile charge carriers include the secondary ion mass-spectrometry (SIMS), the Hall effect measurement (the infrared FTIR-spectroscopy (Fourier Transform Infrared Spectroscopy), the photoconductivity spectroscopy, the capacitance and admittance spectroscopy. Each method is based on specific physical principles and, therefore, it has both advantages and certain disadvantages, which complicate precise and reliable characterization of diamond as the microelectronical material.

The time-of-flight SIMS [87] can be used to measure the complete boron concentration in the sample, but this method is destructive and insensitive to low impurity concentrations. The measurements by the capacitance-voltage characteristics? method ($C-V$) [88] and the galvanomagnetic Hall method [89,90] should be regarded as non-equilibrium ones as they require application of an external electric or magnetic field to the sample. The conditions closest to the thermodynamically equilibrium mode of the measurements provide for the direct current conductance measurements [91,92]. But they are really inferior to modern diagnostics methods in terms of informativity and, in addition, require separate knowledge of the mobility of the charge carriers. Recently, a method of electrochemical capacitance-voltage profiling has proven well to determine the concentration of the majority charge carriers (MCC) in the samples without formed metal contacts [93–96]. But it turns out to be unacceptable for diamond due to inetchibility of this material.

There are works on application of laser spark emission spectroscopy (LIES) for analysis of the impurity composition of the natural and synthetic diamonds [97]. In principle, the LIES method can identify a place of excavation in case of natural diamonds and a growth laboratory in case of synthetic ones.

Here let us describe a comparative characteristic of the physical principles and algorithms underlying the FTIR (the infrared Fourier spectroscopy) and $C-V$ methods and measurement specific features arising therefrom.

### 1.2.1. FTIR-measurements of the impurity concentration

The FTIR-spectroscopy [98] tests the concentration of the optically active impurity boron atoms regardless of whether this atom would contribute to the electrical conductance. The present FTIR spectrum analysis procedure requires using at least three absorption spectrum peaks in order to determine the various concentrations of the boron impurity
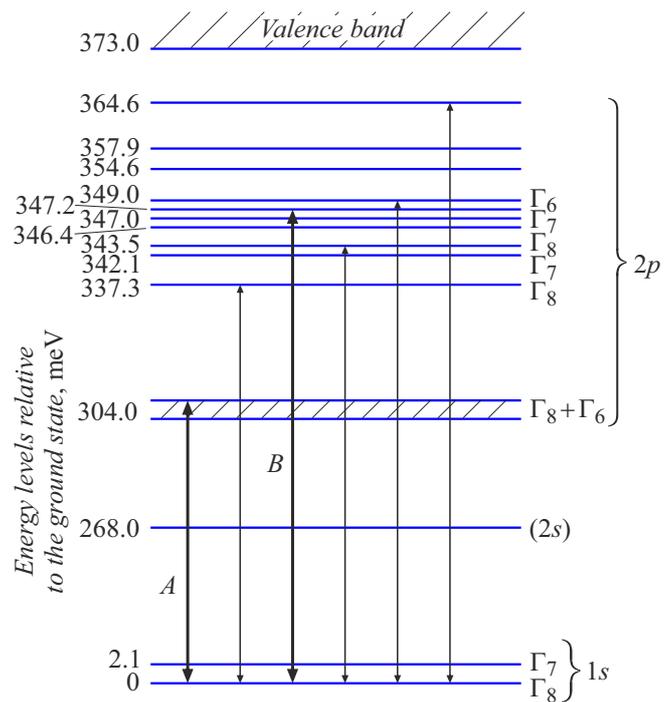


**Figure 3.** Diagram of energy levels of the boron impurity in the weakly-doped diamond (plotted based on the calculations [100] and [59] by the effective mass method). The heavy lines ($A$ and $B$) designate the main transitions observed in the FTIR technique.

in diamond. It usually uses the absorption bands with the wavenumbers 2802, 2454 and 1290 cm$^{-1}$, which are called the primary, secondary and tertiary bands [99]. The peaks 2802 and 2454 cm$^{-1}$ in boron weakly-doped diamond are created by hole transitions from the main $1s$-state to the system of split excited $2p$-states of the acceptor center (Fig. 3). At the same time, the $1s \rightarrow 2s$ transitions turn out to be forbidden. Note that the wave length conforming to 2802 cm$^{-1}$ corresponds to the transition energy of 347 meV. It is a maximum boron activation energy registered in the diamond FTIR spectra.

The heavily-doped samples use the peak at 1290 cm$^{-1}$, as due to emergence of the impurity band the narrow boron responses disappear in the region of intrinsic three-phonon absorption. The tertiary band is in the defect single-phonon region and is relatively weak in comparison with the absorption bands caused by the $1s \rightarrow 2p$ transitions in the weakly doped samples.

As the FTIR spectra are technically measured in a transmission mode, they ensure determination of the sample depth averaged concentration of the partially compensated boron impurity. As it is usually for optics, in order to obtain quantitative results, calibration of intensity of the spectrum peaks is applied, whereas it is separate at various portions of the spectrum. It is calibrated by comparing with the direct methods of concentration determination (SIMS [101], the Hall method, the $C-V$ method). The recent work [99] generalizing multi-year experience of a

team of authors has used the „primary standard" to select the data of the Hall measurements for normalization. Note, however, that the Hall method tests the concentration of the free charge carriers rather than the impurity. And for the wide bandgap diamond such normalization can provide a large (hundreds of percent) systematic error in determination of the impurity concentration, unlike, for example the capacitance-voltage measurements, which do not require the normalization and are direct in this case (for more details see in Section 1.3). When studying the samples with a non-uniform doping level, including the multi-sector samples, this method additionally contributes to the error of the measurement results. In addition, it is obvious that for the high boron concentrations really demanded in the electronic industry, the accepted diagram of the energy levels of the boron impurity (Fig. 3) should be critically revised.

### 1.2.2. Voltage-capacitance characteristics, basic milestones

The capacitance-voltage (or $C-V$) profiling technique is based on quantitative measurement of a charge increment when the voltage changes [88,102–104]. The classical consideration is based on the fact that the local distribution of the ion concentrations of the impurity and the mobile charge carriers determines the increment of the charge $dQ$ itself as well as the increment of the width of the space charge region (SCR) with each change of the value of the reversal shift applied to the structure [105]. By differentiating the $C-V$-dependence with respect to voltage, we get a standard expression for the distribution of the concentration along the sample depth, which is commonly referred to as an observed („apparent") concentration profile [88]:

$$N(w) = \frac{C^3}{e \varepsilon_r \varepsilon_0 S^2} \left(\frac{dC}{dV}\right)^{-1}, \qquad (1)$$

where $e$ — the electron charge, $S$ — the sample area, $\varepsilon_r$ — the relative permittivity, $\varepsilon_0$ — the electrical constant; the thickness of the depleted layer $w$, corresponding to the barrier capacitance $C$ at the given voltage $V$ (designated as $U$) is equal to

$$w = \frac{\varepsilon_r \varepsilon_0 S}{C}. \qquad (2)$$

It is compared with a current coordinate of the SCR boundary at this voltage.

The profile (1) depends in a complicated way on the distribution of the dopant concentration and the location of the edge of the semiconductor energy band. Only in case of the uniform semiconductor, in which the impurity is uniformly distributed and completely ionized, the value determined from (1) can exactly correspond to the doping level [103].

In relation to the instrument structures on the single-crystal diamond, the $C-V$-profiling is potentially a more exact and informative method of diagnostics as compared to

the optical measurements of the concentration. Firstly, the $C-V$-characteristic is used to calculate the distribution of the concentration of the ionized impurity (or the majority charge carriers) along the structure depth rather than the volume-averaged concentration (Table 1). Secondly, the operating conditions of the diamond instrument include the high temperatures and the applied shift, thereby resulting in the changed concentration of the mobile charge carriers in relation to the equilibrium one. Unlike FTIR, the $C-V$ method can characterize the distribution of the charge carriers in the instrument at the operating temperature and actually in real operating conditions.

It is obvious that the specific features in the measurements of the concentration of the impurity and the MCCs, which are shown in Table 1, are true not only for diamond, but for other wide bandgap materials (SiC, $Ga_2O_3$, GaN and its solid solutions GaAlN).
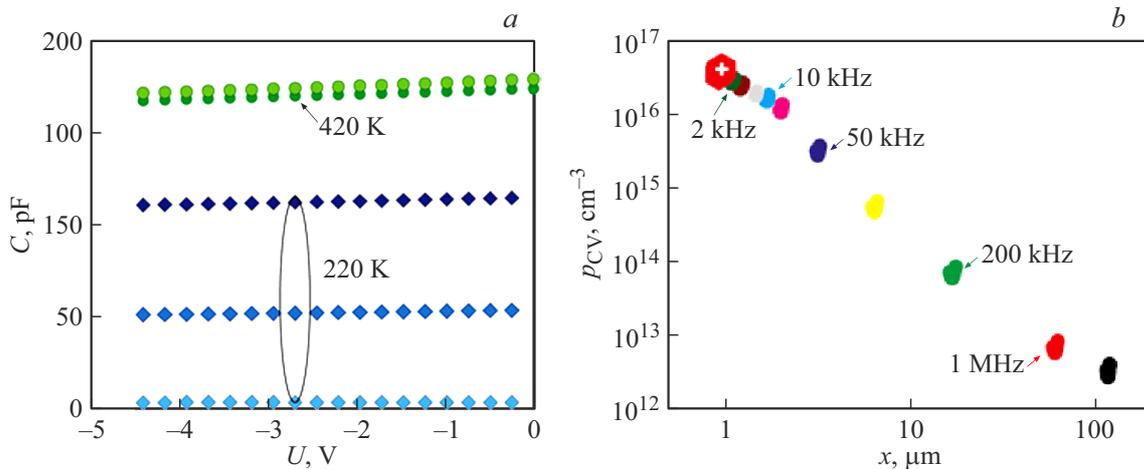
## 1.3. Specific features of the capacitance-voltage measurements of the semiconductor diamond

### 1.3.1. Frequency dispersion of the measured capacitance. Non-quasistatic nature of the $C-V$-characteristics

The strong (in several orders) dependence of the measured barrier capacitance on the frequency is a characteristic feature of the wide bandgap diamond. The cause of this effect is closely related to the low degree of ionization of impurity boron and a low pace of hole emission from this center into the corresponding band. The test alternating voltage applied by a capacitance meter disturbs the equilibrium state of the charge carriers and a capacitance response received from the sample varies with the frequency of the applied shift. This effect is called the capacitance dispersion and causes disruption of the quasi-static nature (i.e. independence on the frequency) of the capacitance-voltage measurements. Accordingly, the „apparent" concentration also turns out to be dependent on the frequency of a forcing signal. For the first time it was observed in diamond at the room temperature by G. Glover [106]. The dispersion of the barrier capacitance increases with the temperature decrease (Fig. 4, $a$). This phenomenon complicates the interpretation of the results and requires using the non-equilibrium statistics of the semiconductors for analysis. Theoretically, the test signal of the very low frequency can emit the maximum charge carriers from the deep center, and the high-frequency measurements will almost unchange the equilibrium distribution of the free holes. Therefore, with corresponding setup of the experiment the measurements of the frequency dispersion of the $C-V$-characteristics can give the quantitative information both about the impurity concentration and the equilibrium concentration of the charge carriers (Fig. 4, $b$) ($p_{cv}$ here — the observed or apparent hole concentration calculated from (1)). The saturation $p_{cv}$ at the low frequencies reflects almost full

**Table 1.** Measured parameters of the impurity and the majority charge carriers in the bulk doped diamond and the methods applied

| Method | Measured parameters | Specific features | |
|---|---|---|---|
| SIMS | Complete concentration of the impurity atoms, $N_{impur}$ | Non-sensitivity to low concentrations | |
| Hall measurements | Major charge carriers, $p-n$ | Quasi-equilibrium conditions | |
| FTIR measurements | The average value of the concentration of the partially compensated impurity, $N_A - N_D$ | Normalization for the Hall measurements | |
| Voltage-capacitance characteristics | Coordinate distribution of the concentration of the ionized impurity taking into account its compensation, $N_A^- - N_D^+$ | Frequency dispersion of the measurement results | |



**Figure 4.** *a* — capacitance-voltage $C(U)$-characteristics of the boron weakly-doped diamond as measured at the temperatures of 220 and 420 K. The measurements are carried out at the frequencies 5, 50 and 500 kHz; *b* — the depth of the concentration profiling at $T = 220$ K as the function of the frequency of a test signal. The hexagon with a cross — the quasi-static concentration at 420 K.

ionization of the impurity in the applied electric field, i.e. it is possible to evaluate the impurity concentration here and it will not depend on the temperature. The high-frequency measurements provide the concentration of the free charge carriers close to their equilibrium concentration at a given temperature. We have previously demonstrated it in [107].

The correlated satellite effect is a dependence of the width of the space charge region (SCR) on the frequency of the test signal at the same applied shift. It is clearly seen on Fig. 4, *b*, where the profiling portion is deepened from fractions of $\mu$m to $100\,\mu$m with increase of the frequency from 1 kHz to 1 MHz. This effect can be easily understood from the perspective of the Gauss theorem about a recharging-involved complete charge $Q$ of the carrier-depleted region [103,105]:

$$\frac{1}{\varepsilon_r \varepsilon_0} QS = -\mathbf{E}_s S, \qquad (3)$$

where $\mathbf{E}_s$ — the value of the field intensity at the sample surface (at $x = 0$). For the single-dimension case $\mathbf{E}_s$ actually corresponds to the potential difference applied to the structure. The less ionization degree of the impurity, the

less formed charge and the wider SCR is taken to collect it for compensation of the applied voltage.

### 1.3.2. Abnormally large cutoff voltage

The consequence of the phenomena described in the previous sections is the abnormally large cutoff $C-V$ voltage. As demonstrated by the measurements, for the boron weakly- and moderately-doped diamond it can be from 50 to 200 V at various frequencies depending on the doping level (Fig. 4, *a*). It seriously contradicts the classical model $C-V$, which correlates the cutoff voltage to the contact potential difference at the metal-semiconductor barrier. At the same time, a very small experimentally-obtained slope of the curve $1/C^2 - V$ (fractions of fF/V) imposes higher requirements to the sensitivity of the measurement equipment.

In terms of a circuit of connecting the sample to the recording equipment, this behavior of the capacitance-voltage characteristics of diamond is explained by the large consecutive resistance $R_S$ of the sample bulk due to weak ionization of the impurity. This resistance is a non-linear function of the temperature and, in addition, it varies under
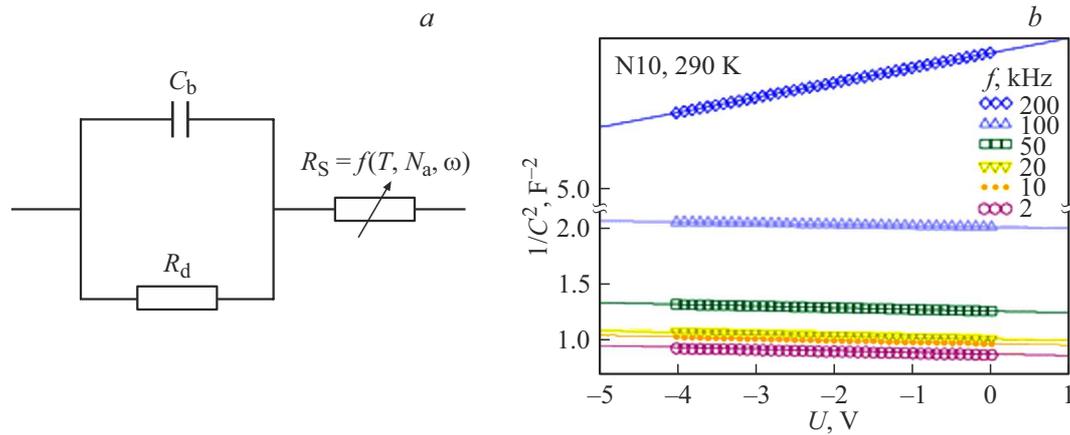
**Figure 5.** *a* — the equivalent diagram of the Schottky barrier with diamond; *b* — measured (symbols) and calculated (solid lines) capacitance-voltage characteristics of the sample at $T = 290$ K.

impact of the shift applied to the sample. Generally, the equivalent sample diagram is at least a series-parallel circuit of a common barrier capacitance of the Schottky diode $C_b$, its shunting differential resistance of the space charge region $R_d$ and the series-connected alternating resistance of the basic region $R_S$ (Fig. 5, *a*).

In the measurements, the RLC meter reduces the full equivalent diagram into the two-element parallel or series one. In a typical case of the $C-V$-measurements of the semiconductor with the completely ionized impurity, when $R_S$ does not depend on the temperature and the true barrier capacitance $C_b$ is distorted only due to leakage currents through the SCR (which is determined by the value $R_d$), the differential capacitance measured by the instrument with the specific shift is determined as [103,108,109]:

$$C_m = C_b \frac{R_d^2}{(R_d + R_S)^2} \frac{1}{1 + [(\omega C_b R_d R_S)/(R_S + R_d)]^2}, \quad (4)$$

where the proper barrier capacitance

$$C_b(T) = S\left(\frac{\varepsilon_r \varepsilon_0 e N_A^-(T)}{2(V - V_{bi})}\right)^{1/2}, \quad (5)$$

$T$ — the temperature, $V_{bi}$ — the contact potential difference; $N_a^-$ — the concentration of the ionized acceptor impurity (boron).

In the real measurements of the semiconductor with the partially ionized impurity the capacitance $C_m$ depends on the applied shift and the frequency both through the respective change $C_b$ and through $R_d$ and $R_S$ as well. It results in the substantial difference of the characteristic $C_m^{-2}(V)$ from the characteristic $C_b^{-2}(V)$, as shown on Fig. 5, *b*. So, with increase of the resistance $R_S$ and the test frequency of a measurement signal $\omega$, the characteristic $C_m^{-2}(V)$ is initially shifted in parallel along the the ordinate axis upwards; with their further increase the characteristic slope decreases and further on it can even change to the

opposite one in accordance with the formula [110]:

$$\frac{p_{cv}}{p_{true}} = \frac{1}{(1 - \omega C_m R_S)^4}. \quad (6)$$

At the same time, the cutoff voltage alters the sign. In accordance with it, the „apparent" concentration $p_{cv}$ determined as per (1) will substantially differ from the true charge carrier concentration $p_{true}$ and can even become negative, which is obviously an artefact. We have discussed this effect in the work [107] in relation to the electrochemical measurements of the wide bandgap semiconductors.

For the routine $C-V$ measurements of the impurity concentration in the wide bandgap semiconductor a practical solution is to use the low frequencies and the high temperatures with control of the cutoff voltage. On the other hand, modelling of the experimentally-observed (apparent) capacitance $C_m^{-2}(V)$ with fitting to the measured frequency-dependent $C-V$-characteristics can carefully determine desired characteristics of the sample [103,111].

### 1.3.3. What is determined by the $C-V$-measurements: the concentration of the dopant or the concentration of the majority charge carriers?

The diamond being the wide bandgap semiconductor ($E_g = 5.45$ eV) has a high ionization energy $E_A$ of the boron impurity (for the boron weakly-doped diamond the reference value is $E_A = 370$ meV [112,113]). Therefore, an experimentally-available temperature range is mainly within the portion of the impurity electrical conductivity. At these temperatures, only a small portion of the boron atoms (as noted, below 1%) turns out to be ionized. In this regard, the $C-V$-measurements of the semiconductor diamond include determination of the concentration of the non-equilibrium free charge carriers, which obviously turns out to be the temperature-dependent one. And its value (except for the measurements at the higher temperatures)

will be less than the concentration of an electrically-active impurity $N_A$, but higher than the thermodynamically-equilibrium concentration of the free charge carriers $p_0$. It is caused by the reversal shift applied to the sample during the $C-V$-measurements, which contributes to the additional ionization of the impurity [114]:

$$N_A^-(x) = \frac{N_A}{1 + g_A \exp\left[(E_A - E_F - e\varphi(x))/kT\right]}, \quad (7)$$

where $g_A = 6$ — the factor of degeneracy of the energy level $E_A$ of boron in diamond taking into account a spin-orbit weakly-split band for holes [115]. Here $E_A$ the energy of the Fermi level $E_F$ are read from a ceiling of the valence band, $\varphi(x)$ — the electric potential.

The induced potential available at the temperatures above the room one results in almost full ionization of the impurity, and the experiment exhibits no dependence of the „apparent" concentration on the temperature. Without the large error, it can be assumed that in these conditions the concentration of the electrically active impurity is measured (we have studied the similar in GaAs [111,116]). At the same time, at the temperatures below the room one the „ad-ionization" of the charge carriers by the field is weakening and the difference between the „apparent" and thermodynamically equilibrium concentration of the charge carriers amounts to at least two orders, as shown on Fig. 4, *b*.

This problem is described with more details below when considering the dependence of the energy of the thermal ionization of the boron impurity on its concentration in diamond.

## 1.4. Methods of measurements of the impurity activation energy. Quasi-static and dynamic temperature spectra of the conductance

### 1.4.1. Measurements of the temperature dependence of the direct current conductance

The temperature-dependent direct current conductance (DC-conductance) seemed to be the historically first control technique among the electrophysical methods of measuring the impurity activation energy. An attractive feature of the method is a simple measurement arrangement and the similarly simple physics based on the conductance expression $\sigma(T) = en(T)\mu(T)$, where the concentration of the free charge carriers $n$ (or $p$) exponentially depends on the temperature, so does their drift mobility as per a much weaker law of the kind $\mu(T) \sim T^s$, where $0 < s < 2$. Just the first measurements of the conductance (or resistance) of germanium in the wide temperature range [117,118] had revealed several (up to three) linear portions of a different slope at the dependence $\ln\sigma = f(1/T)$, which was later confirmed many times by the measurements at various semiconductors, including on diamond. [92,119]. It is exemplified on Fig. 6.
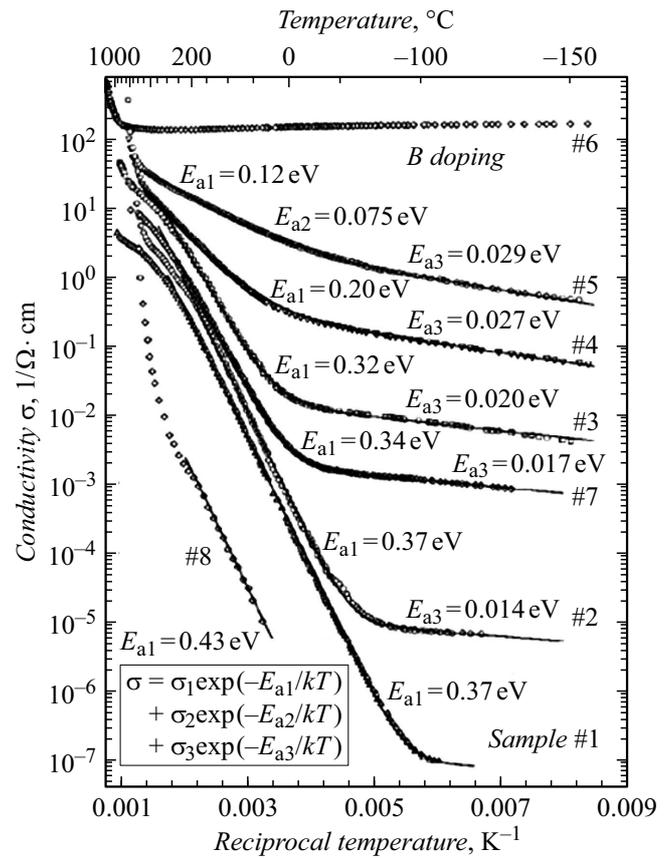


**Figure 6.** Temperature dependence of the impurity conductance in boron-doped diamond. Originally reprinted from [119].

The traditional interpretation of the results of the measurement of the DC conductance involves three mechanisms of emission of the charge carriers for separate portions:

1) common ionization of the charge carrier from the impurity center (which is an acceptor one in case of boron in diamond) into the corresponding band of delocalized states (a valence band), which is characterized by the energy $E_{A1}$;

2) motion of the charge carriers along neutral acceptors („seldom observed impurity-band conduction with a motion of carriers over neutral acceptors") [119] with the activation energy $E_{A2}$;

3) hopping conduction for the impurity band with the activation energy $E_{A3}$, which is observed at the low temperatures and the high impurity concentration:

$$\sigma(T) = \sigma_1 \exp(-E_{A1}/kT) + \sigma_2 \exp(-E_{A2}/kT)$$
$$+ \sigma_3 \exp(-E_{A3}/kT). \quad (8)$$

The empirical formula (8) involves a piecewise-exponential dependence of the conductance on the temperature. Although in the compensated semiconductor the concentration of the charge carriers in the low-temperature region depends on it in a more complicated way (Fig. 7). In
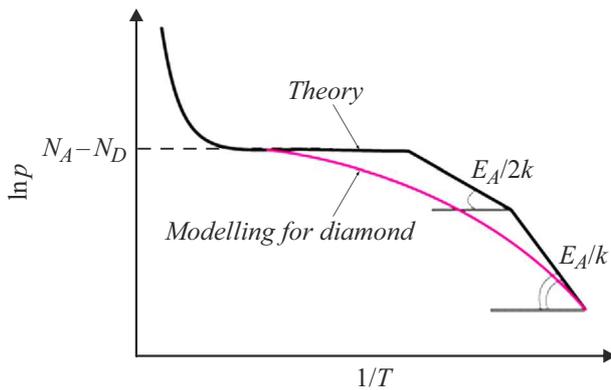
**Figure 7.** Temperature dependence of hole concentration $p$ in the compensated semiconductor.

addition, (8) does not take into account various dissipation mechanisms in the temperature dependence of the mobility.

J.-P. Lagrange [120] has interpreted the activation energies of (8) in line with classical statistics of the semiconductors [121], which selects two portions in the low-temperature part of the impurity conductance of the compensated semiconductor (Fig. 7). He has fitted his experimental dependences based thereon. He has obtained the activation energy of 368 meV within the temperature range $300-500$ K and half the activation energy (185 meV) at the temperatures $500-1000$ K. The last statement should be obviously considered as a mistake. Within the framework of approximations adopted here, it is just changing the formulae for the concentration of the free charge carriers (holes) at the various portions with implying the change of the method of determination of $E_A$, but not the change of the activation energy itself.

It is more correctly to exactly solve the full non-linear equation of the electrical neutrality for the partially compensated semiconductor:

$$n(x, T) + N_A^-(x, T) = p(x, T) + N_D^+(x, T) \qquad (9)$$

taking into account the spatial distribution of the concentration of the acceptor $N_A$ and donor $N_D$ impurity in reference to the coordinate $x$. Within the framework of this solution, the low-temperature part of the impurity conductance is never described by the exponent (Fig. 7, the red curve (in the online version)). Therefore, there are no grounds to introduce $E_A/2$. Obviously, it should not be interpreted as the gradual change of the activation energy of the impurity with the temperature reduction as well.

The hopping conduction of the charge carriers for the impurity band will be discussed by us below in Section 2.6.

### 1.4.2. Temperature and frequency admittance spectra

The admittance (or the full conductance) is a complex magnitude characterizing the electric circuit or instrument's capability of conducting the current under impact of the applied alternating voltage of a given frequency $f$ [103]. The admittance is measured using RLC meters or immittance measuring instruments. The immittance is a generic name for admittance and impedance (for the complex resistance). A measuring system in the instrument is balanced simultaneously by the capacitance and active components of the admittance $Y$:

$$Y = 1/Z = G + jB, \quad G = 1/R, \quad B = 2\pi f C,$$

where $G$ — the active part of the admittance — conductance, $B$ — the capacitance part (susceptance), $R$ — the resistance, $C$ — the capacitance. The magnitude reciprocal to the admittance, i.e. the impedance $Z$, has an active and capacitance part, too. As the semiconductor diode is a fundamentally non-linear system, the immittance measuring instrument selects the response only at the frequency of the forcing signal [103,122] by filtering all other components of the output signal.

The admittance of the semiconductor instrument is determined by its electron spectrum. Therefore, its value depends on the temperature $T$, the voltage $V$ applied to the structure and the frequency of the measurement signal.

In accordance with the theoretical representations of the admittance spectroscopy, when applying a small alternating signal to the sample with a deep trap with the activation energy $E_A$, the speed of emission of the charge carriers into the corresponding band (in this case it is the valence band) is described by the expression [88,122]:

$$e_p = g_A v_{th} \sigma_p N_V \exp(-E_A/kT) \equiv AT^2 \exp(-E_A/kT), \qquad (10)$$

where $N_V$ — the effective density of the states in the valence band, $v_{th}$ — the thermal speed of the holes, $\sigma_p$ — the hole capture section, $g_A$ — the degeneracy factor of the acceptor level; the pre-exponential multiplier $A$ is virtually independent of the temperature.

The temperature frequency methods of the admittance spectroscopy focus only on the alternating shift current at the assigned frequency $\omega$ in neglecting the leakage current through a rectifying transition. At the same time, the recorded conductance signal is of a resonance nature [123,124]:

$$G(\omega, T) = \frac{e_p(T)\omega^2}{e_p^2(T) + \omega^2} \frac{N_T}{p} C_b(T), \qquad (11)$$

the maximum conductance spectrum $G$ is achieved at $e_p(T) = \omega$ [103]. Here $N_T$ — the concentration of the deep centers in the band gap involved in the recharging, $p$ — the concentration of the delocalized (free) holes in the valence band,

$$C_b(T) = S \left( \frac{\varepsilon_r \varepsilon_0 e N_A^-(T)}{2(V - V_{bi})} \right)^{1/2}$$

— the quasi-static barrier capacitance of the sample at a specified voltage $V$, $N_A^-$ — the concentration of the ionized acceptor impurity (boron).

### 1.4.3. Dependence of the activation energy of the boron impurity on the concentration

The fundamental requirement to the semiconductor diamond means doping it with an electrically active impurity to the high concentrations. Here, exactly, one of its key features is manifested and it is unessential in the common semiconductors such as Si and GaAs — i.e. sharp reduction of the activation energy with increase of the boron concentration, as accompanied by the transition to the hopping conduction [92]. Generally, this effect is described by the Pearson-Bardeen theoretical dependence [125]:

$$E_A = E_I - \alpha N_A^{1/3}, \qquad (12)$$

taking into account the potential energy of attraction of the free charge carrier to an ion, which increases with decrease of the average distance between the impurity centers. here $E_I$ — the energy of ionization of the isolated impurity center, $\alpha$ — the constant determined by properties of a specific semiconductor. Later, the authors [119,126] had established the parameters in the formula (12) for the boron impurity in diamond with a low degree of compensation and they were confirmed by Lagrange [120]:

$$E_A = 0.37\,\text{eV} - 6.7 \cdot 10^{-8} N_A^{1/3} \; [\text{eV} \cdot \text{cm}]. \qquad (13)$$

In addition, the ionization energy is decreased with increase of the impurity concentration due to emergence of state density tails in the energy band gap and smearing of the impurity band [127]. In our measurements, we have observed the reduction of the boron activation energy from 325 to 100 meV with increase of its concentration from $3 \cdot 10^{16}$ to $4 \cdot 10^{19}\,\text{cm}^{-3}$. It will be considered in detail in Section 2.7 based on the experimental data.

Note that this effect also has a positive side, i.e. the reduction of the activation energy ensures the higher degree of the impurity ionization. And, in turn, it substantially facilitates producing the operating concentrations of the free charge carriers in the diamond-based instruments. This behavior of the boron impurity is fundamental for this wide bandgap material and, obviously, it is of great practical importance.

### 1.4.4. Differences of the activation energy from the constant and alternating current measurements of the conductance

The literature has a few number of articles dedicated to admittance (as well as non-stationary capacitance) measurements of diamond. Previously, they have been performed mainly on polycrystalline samples [101,128–131]; in doing so, the activation energies $E_A$ were obtained for boron within the range $300-360$ meV.

In the works [84,132,133] we have for the first time performed a systematic cycle of the admittance measurements on the samples of boron-doped single-crystal diamond. The admittance spectra of the weakly-doped diamond samples with the boron concentration $N_A = (2-5) \cdot 10^{16}\,\text{cm}^{-3}$, which are measured at the alternating (AC) test signal, give the typical activation energy of the boron acceptor level within the range from 285 to 325 meV [133]. This value is substantially lower than a reference value of the optical ionization of the boron impurity 0.373 eV (as obtained by means of measurements of the direct current photoconductivity [100]) and lower than the activation energy 0.37 eV determined by the direct current measurements of the electric conductance [119,120,134]. It is due to substantially different measurement methods as well as a different algorithm of determination of the ionization energy. As mentioned above, the admittance spectroscopy is a non-equilibrium procedure. The alternating test voltage of the RLC measuring instrument „makes" the deep level recharging in the alternating field and an instrument shall be used to measure charge carriers which are in time for recharging for the duration of the signal period and create a displacement current in the external circuit (Fig. 8). In doing so, the sample responds to the test signal in a semiconductor region localized near intersection of the location of the Fermi quasi-level with the observed deep level. Depending on the ratio of the speed of emission $e_p$ and the frequency of the test signal $\omega$, the degree of the level depletion varies, thereby resulting in a different value of the measured barrier capacitance.

In the direct current measurements of the conductance (or resistance) the thermodynamically equilibrium free charge carriers are accumulated to ohmic contacts in the electric current mode when applying a small pulling field. These measurements are the closest to the equilibrium ones. It can be assumed that the differences of the activation energies obtained by the different methods are caused by the measured displacement or electric currents. In addition, $E_A$ by the DC conductance (on the direct current) is determined based on fitting of the experimental curve $\sigma = f(1/T)$ by a certain model, whose fitting parameters, except for $E_A$, include the mobility of the charge carriers, thereby imparting the additional uncertainty to the uncertainty result.

There is another source of ambiguity of the measurements beside the alternating test signal. The admittance spectroscopy does not include application of the shift to the traditional bulk semiconductors, because the measurement result does not depend on it [135]. Unlike it, the spectra of the admittance of the quantum-dimensional structures are strongly modified due to the shift as caused by impact of the applied electric field on the energetic location of the locally positioned levels and on their ionization degree [136–139]. Due to weak ionization of the impurity, the similar effect is also implemented in diamond. The reversal shift applied to the sample contributes to the additional ionization of the
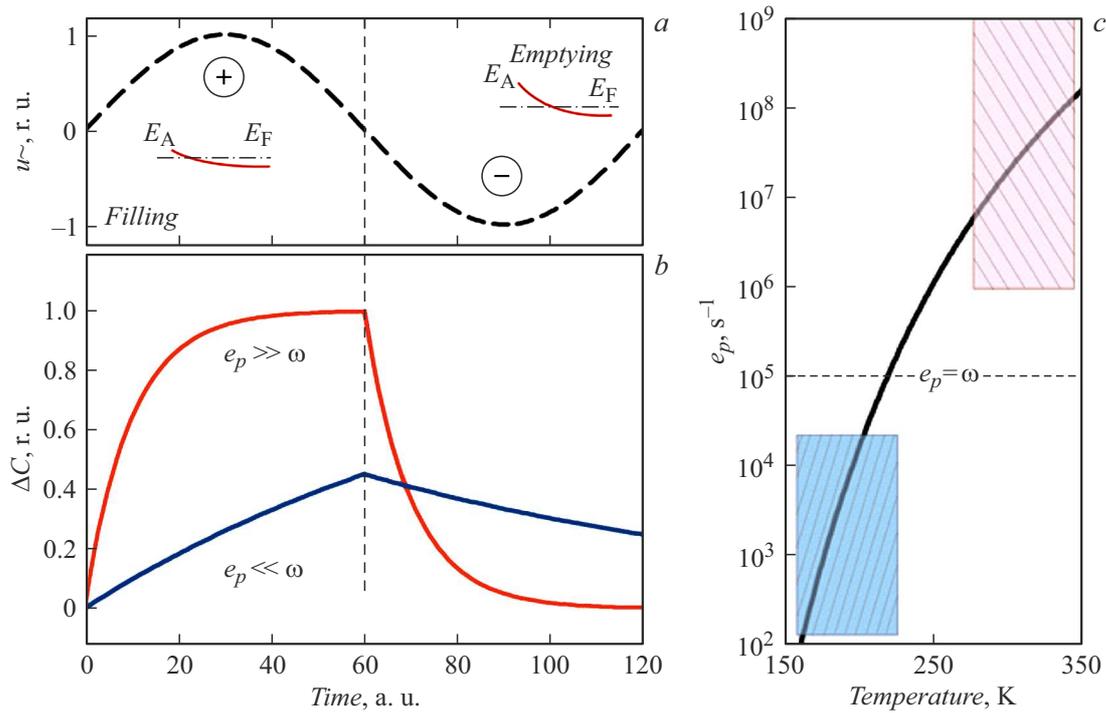
**Figure 8.** *a* — two half-waves of the test signal of the frequency $\omega$ of the RLC measuring instrument; *b* — the respective relaxation of the deep center charge at the various ratio of $e_p$ and $\omega$; *c* — the speed of emission of the charge carriers from the boron function as the temperature function (calculated for the weekly-doped sample).

impurity:

$$N_A^-(x) = \frac{N_A}{1 + g_A \exp\left[\left(E_A - E_F - e\varphi_{DC}(x) - e\varphi_{AC}(x)\right)/kT\right]}, \tag{14}$$

thereby resulting in the reduced recorded (observed) activation energy. The expression $E_A - e\varphi_{DC}(x)$ of (14) can be interpreted as the reduced effective activation energy in the admittance method.

Finally, note that the measurements in the admittance spectroscopy method most closely correspond to the operating conditions of the semiconductor instrument. And we assume that it is these dynamic activation characteristics which should be expected for real diamond instruments.

## 2. Experimental results

### 2.1. Measurement methods and equipment

The key diagnostics method of the present work is the admittance spectroscopy, which has a number of indisputable advantages as compared to others. It is a non-destructive method, which can be used to carry out the precision quantitative measurements of the dynamic characteristics of an ensemble of the charge carriers and the impurity centers for predicting the instrument properties. The resonance-charge nature of the measurements can give exact values of the activation energy, the speed of emission/capture, the capture section and other properties of the impurities and

the traps [103]. At the same time, in terms of its physical basics the admittance spectroscopy should be regarded as the non-equilibrium measurement technique, as it requires application of the alternating test signal causing recharging of the energy levels and sometimes it is also accompanied by the reversal shift of the structure. For the measurements of semiconductors typical for the microelectronics (Si, Ge, GaAs) with the impurity fully ionized at the room temperature, this measurement non-equilibrium does not result in complications in interpretation of the results obtained [88,102,135,140]. In case of substantially underradionized dopant (boron in diamond) the experiment result will strongly depend on the selection of the measurement parameters (frequency, temperature), as we have discussed in the first part of the review. These problems seriously complicate the interpretation of the experiment results and require detailed analysis.

We have measured the samples with applied metal contacts using an automated complex of the admittance spectroscopy [132,141,142]. It includes the cryogenic probe station Janis CCR-10 (Fig. 9), the temperature controllers LakeShore 336 and LakeShore 331, the precision LCR-meter Agilent E4980A, the vacuum station Pfeiffer D35614. The complex is designed to measure the semiconductor structures within the range of the temperatures $T = 15-475\,\mathrm{K}$, the applied shifts $V \leq 40\,\mathrm{V}$ and the frequencies of the test signal $\omega/2\pi = 100\,\mathrm{Hz}-2\,\mathrm{MHz}$.

The developed original algorithms can in one temperature scan collect a multidimensional array of data for capacitance
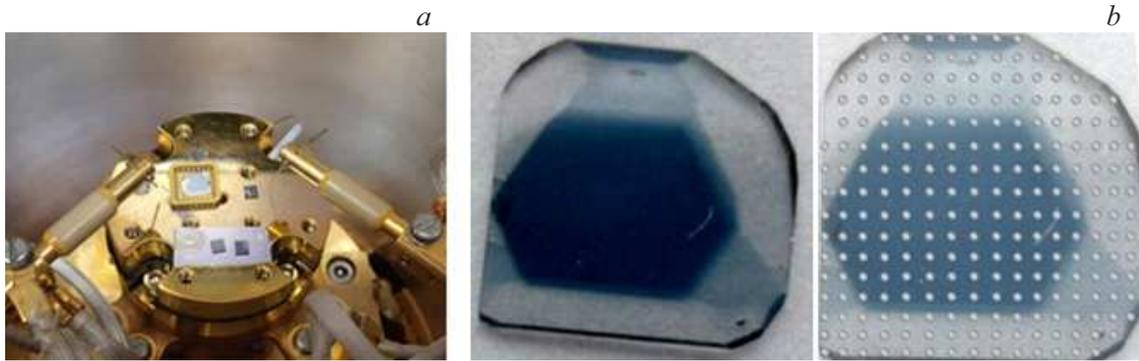
**Figure 9.** Samples being measured: $a$ — in a measurement chamber of the cryogenic probe station; $b$ — the multi-sector diamond plate IL5 before (the left) and after (the right) deposition of the contacts.

and conductance $C$, $G = f(T, V, \omega)$ to be used for drawing up the temperature and frequency spectra.

In order to carefully measure, we have scanned the samples by the temperature with the low speed $0.5 - 1$ K/min, minimizing the possible sweep hysteresis with increase and decrease of the temperature. The spectra of the sample conductance have been measured within the entire available range of frequencies and temperatures in vacuum of at most $10^{-6}$ mbar.

## 2.2. Studied samples

The studied object was a set of the single-crystal samples of boron-doped diamond, of a various nature: natural, epitaxial CVD layers, bulk single- and multi-sector HPHT plates. The preliminary morphology of the sample surface was studied using an atomic-force microscope (AFM) SOLVER NEXT produced by NT-MDT. The diamond surface was scanned by selected special diamond-coated conducting probes.

### 2.2.1. HPHT plates

The studied plates were produced from diamond crystals grown by the HPHT method in LLC „New Diamond Technology" and doped by boron during the growth. The crystals were grown out of cuboctahedral seadings of sizes $0.4 - 0.5$ mm with the crystal faces $\langle 111 \rangle$. The growth took $10 - 14$ days at the temperature of $1400°C$, and the weight of the grown crystals was $8 - 15$ carats. Boron was added in a weighed amount directly into a growth cell. The concentration of the impurity depended on the weight of boron placed in the chamber. The samples were a number of parallel plates cut perpendicularly to the [111] or [001] crystal-lattice directions and sized from $3 \times 3$ to $5 \times 5$ mm and having the thickness of $0.3 - 0.5$ mm (Fig. 2). The samples were both the single-sector and multi-sector ones and colored from transparent lightish-blue to dark-blue. In particular, the sample IL1 — is a transparent single-sector one sized by $3.5 \times 3.5$ mm. The sample IL5 — the multi-sector sized by $5 \times 5$ mm with three distinct regions: the

blue one (B) with the [111] orientation, the light blue one (L) [110] and the transparent one (T) [100] (Fig. 9, $b$). The sample IL4 — the multi-sector plate with a heavily-doped blue region (B) with orientation along the [111] direction and the transparent region [100] (T) (Fig. 10, $a$). The plate is sized as — $3 \times 3$ mm.

The AFM scans of the synthesized diamonds exhibited traces in two directions. The arithmetic mean roughness was at most $15$ nm among all the synthesized diamonds. This surface quality allows reliably performing the post-growth technological operations, including application of the contacts [84]. The HPHT plates got the best morphology among the studied samples, and their roughness was $1 - 3$ nm (Fig. 10, $b$–$e$).

### 2.2.2. CVD-epitaxial layers

The boron-doped diamond layers were grown in IPF RAS on the (100) HPHT-diamond plates. They were grown in a cylindrical MPACVD-reactor with the operating frequency of $2.45$ GHz [45,46], which had the mixture of working gases $H_2 + CH_4$. The different doping levels were obtained by using solutions with various concentrations of trimethyl borate in ethanol ($2 - 16\%$) and by varying the power of the gas flow through a bubbler as well ($4 - 16$ cm$^3$/ min). The boron-carbon ratio of the gas phase (B/C) varied from $600$ to $12\,000$ ppm. The samples were sized as $3 \times 3$ mm, while the thickness of the epitaxial layer was $2 - 2.7\,\mu$m.

### 2.2.3. Natural crystals

The samples of the light blue natural diamonds were temporarily provided for the measurements by the Smithsonian Institution of Washington, USA. The samples were not faceted and they were variously shaped crystals polished at two sides. The shape of the Apollo Blue sample is close to the parallelepiped with the edges of $4$ mm and the height of $2$ mm (the weight $1.127$ ct). The linear dimensions of the Steinmetz sample were approximately in $1.2$ times less (its photo is shown on Fig. 11). The flat side of the samples was used to deposit the contacts, and special mandrels
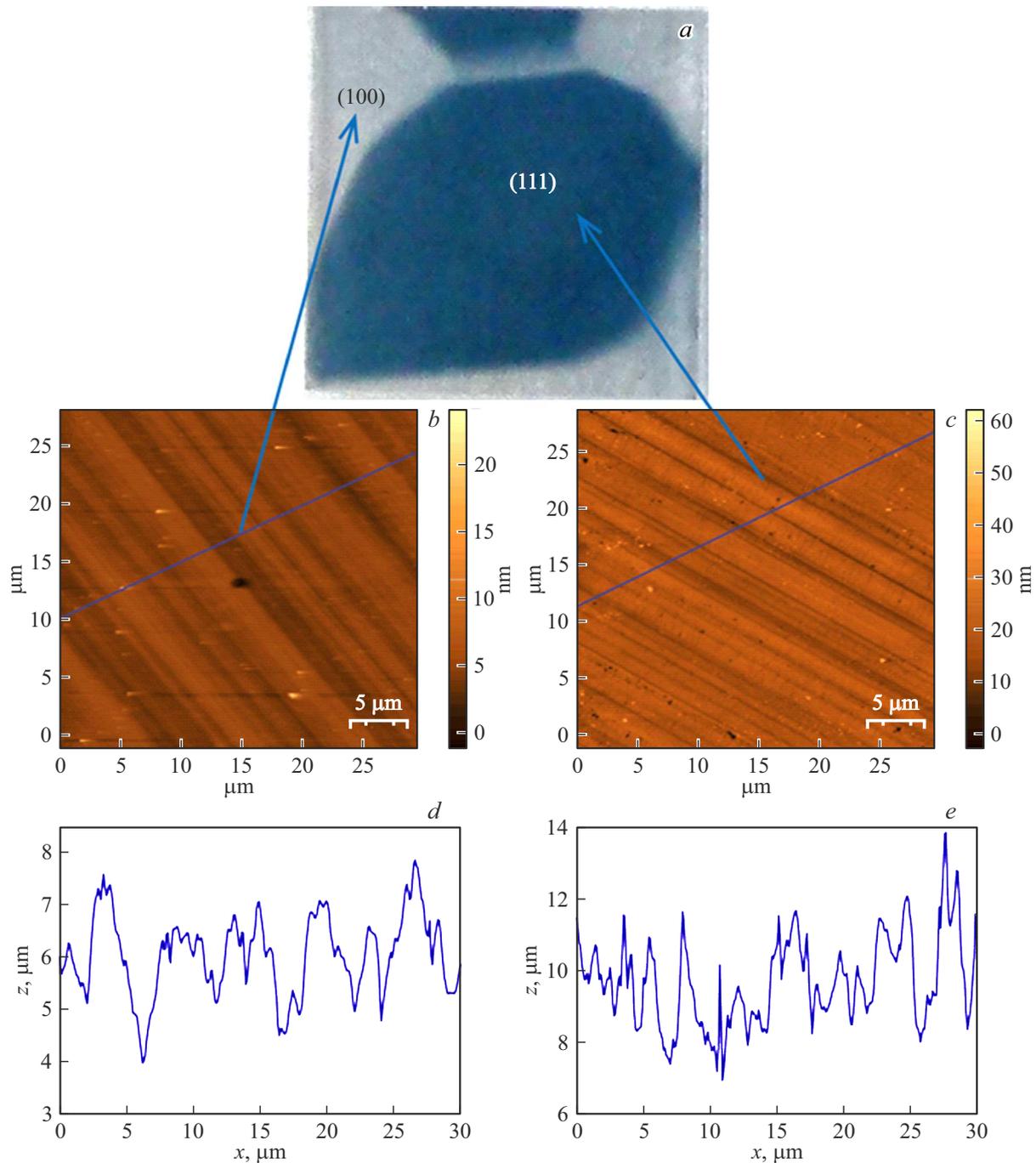
**Figure 10.** Sample IL4: $a$ — the photo, the AFM scan of the surface and the profile along the specified line for the transparent $(b, d)$ and blue $(c, e)$ region.

were manufactured to fix them and carry out the electrical measurements in the probe station.

The surface roughness of the natural diamonds studied in the present work has been evaluated to be more than 250 nm, and more often, units of $\mu$m. We have studied these samples earlier in [143] for relation between the diamond origin and its physical characteristics. Therefore, they were polished only to apply the contacts for carrying out the electrical measurements.

## 2.3. Characterization of the diamond samples

In this part of the work we will fix on discussion of problems and features in determination of the concentration of the majority charge carriers in the single-crystal diamond using the method of the capacitance-voltage characteristics. We will compare the concentrations $p_{CV}$ obtained from the $C-V$ measurements with the optical FTIR measurements.
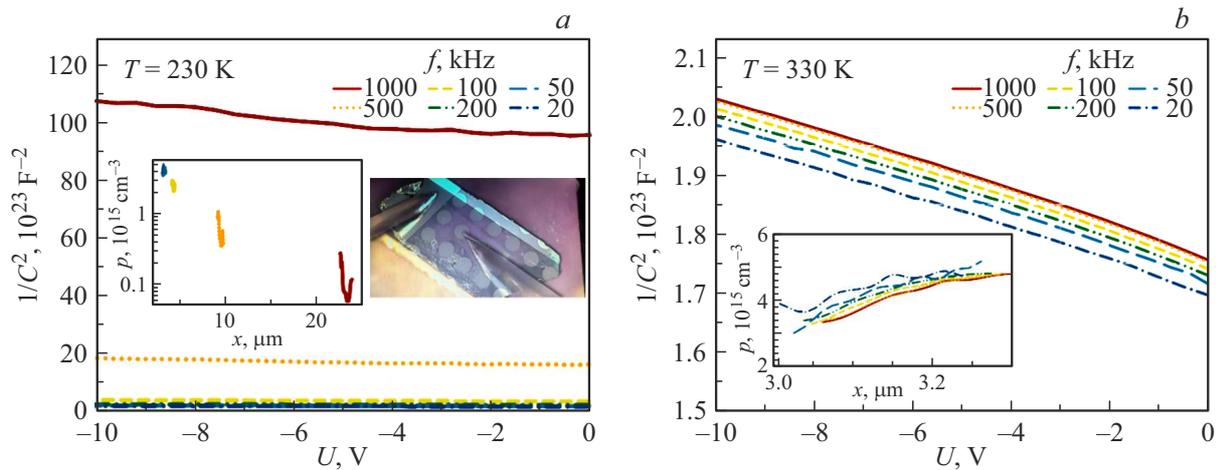
**Figure 11.** The capacitance-voltage $C(U)$ characteristics of the Steinmetz sample and the calculated concentration profiles (on the inserts) for the various frequencies of the test signal at the temperatures: $a$ — 230 K, the strong frequency dispersion; $b$ — 330 K, the weak frequency dispersion.

### 2.3.1. Electrical contacts

The capacitance-voltage measurements require manufacturing of the metal contacts to the sample. The existing literature has been analyzed to show a large variability in selecting the metals and the contact application technology for carrying out the electrical measurements. In order to make the ohmic and rectifying contacts to diamond, we have selected platinum, which was deposited using the magnetron spraying method. For the bulk-doped samples, the vertical geometry of the Schottky diodes was selected, for the epilayers — the planar arrangement for the Ohmic and Schottky contacts. The ohmic contacts were annealed at $300°C$ and the rectifying contacts were deposited at $70°C$ through a mask of the diameter of $130\,\mu m$. Unconditionally, the single-layer ohmic contact is not perfect in terms of getting low resistance for the instrument application, but when applying the reversal shift it can quite satisfactorily carry out necessary capacitance measurements.

### 2.3.2. I-V characteristics

The electrical characteristics of the samples were measured within the wide range of the temperatures using the automated complex of the admittance spectroscopy.

In the weakly-doped samples, the currents of the reverse branch of the current-voltage curve did not exceed 10 nA when increasing the reversal voltage to $-80$ V. With increasing the concentration of the interstitial boron impurity, at the lesser reversal voltages the significant currents occur. For all the samples, the opening voltage was $2-2.1$ V, and at the ohmic portion of the direct portion of the current-voltage curve it was dozens-hundreds of $k\Omega$.

At the temperatures below 150 K, the direct shift exhibited a weak current (below 1 nA) as a consequence of low ionization of the dopant and absence of intrinsic charge carriers - here diamond behaves as a typical dielectric.

When the temperature is increased, rectifying properties of the Schottky barrier are manifested. At the same time, when achieving the reversal voltage of 10 V, there is a current, which is comparable to the direct branch current. This trend is typical for the wide bandgap semiconductors and enhanced with temperature increase.

### 2.3.3. Voltage-capacitance characteristics

The capacitance-voltage measurements were carried out in a wide range of the temperatures and the frequencies. When recording the $C-V$, the shift interval was selected in accordance with a region of the current-voltage curve, in which the active current component does not contribute significantly to the measured admittance. The applied constant shifts were typically ranged from $-1$ to $0$ V with a step of $0.05$ V for the moderately-doped samples. The weakly-doped samples were measured at the voltages of up to $-10$ V. The alternating current test signal had the amplitude of $30$ mV. The measured characteristics have shown that as a rule the said voltage range exhibits a linear type of the dependence $1/C^2$, which is indicative of uniform distribution of the charge carriers along the structure depth (Fig. 11).

The diamond $C-V$-characteristics were analyzed to demonstrate the availability of the fundamental features when carrying out the measurements in this material. At the temperatures above 330 K the dependences $1/C^2-V$ are close to each other at the various frequencies, while the concentration calculated by them turns out to be the same within the experimental error (Fig. 11, $b$). At the room and lower temperatures, there is a difference of several orders in the capacitances measured at the various frequencies (Fig. 11, $a$). In this regard, the classic theory of the capacitance-voltage profiling (which is based on the concept of „the quasi-static approximation" and is true for

**Table 2.** Characteristics of some studied samples. Comparison of the concentration measurement results in the $C-V$ and FTIR methods

| Sample | Steinmetz | Apollo Blue | B12 | B8 | N10 | IL1 | IL4, sector | | IL9, sector | | |
|---|---|---|---|---|---|---|---|---|---|---|---|
| | | | | | | | T | B | T | L | B |
| Origin | Natural | Natural | CVD | CVD | CVD | HPHT | HPHT | | HPHT | | |
| Thickness of the doped layer $h$, $\mu$m | | | 2.7 | 2.0 | 2.7 | 500 | 300 | | 300 | | |
| $N_A - N_D$ from FTIR, $10^{18}$ cm$^{-3}$ | 0.02 | 0.03 | 2.3 | 1.2 | 0.9 (14*) | 0.048 | – | 21 | – | 2 | 10 |
| $p$ from $C-V$, $10^{18}$ cm$^{-3}$ (300 K) | 0.004 | 0.025 | 4 | 6.2 | 1.4 | 0.035 | 2 | 20 | 0.5 | 3 | 12 |

N o t e * SIMS measurements. The table has dashes for portions, which are small-sized to be focused by the Fourier spectrometer. The regions are designated as follows: B — blue, L — light blue, T — transparent.
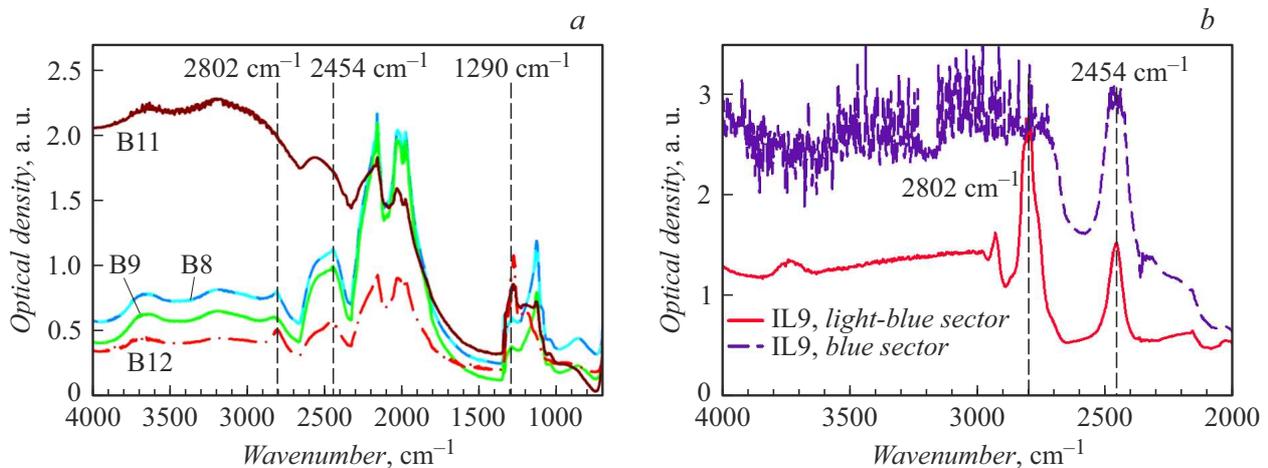


**Figure 12.** FTIR spectra of the sample absorbance with a various degree of boron doping: $a$ — CVD-epilayers, $b$ — HPHT-plates.

the common non-wide bandgap semiconductors [88,140]) is incorrect in this case. We have analyzed consequences of this effect in Section 1.3.1. The authors of [46] have explained the frequency dispersion of the capacitance by the large consecutive resistance $R_S$. Note that the large $R_S$ in the diamond samples turns out to be a consequence of the large energy of hole ionization from the deep boron level, as it is truly specified, for example, in [101].

The concentration profiles of the majority charge carriers at the various temperatures and frequencies have been obtained by differentiating the $C-V$-characteristics as per the formula (1). By the measured hole concentration, all the samples can be divided into the 3 types: the weakly-doped ones $(0.1-6) \cdot 10^{17}$ cm$^{-3}$, the moderately-doped ones $(0.6-6) \cdot 10^{18}$ cm$^{-3}$, the heavily-doped ones $(0.6-7) \cdot 10^{19}$ cm$^{-3}$. With increase of the temperature, the hole concentration increases. This difference is quite noticeable for the heavily-doped samples in the available range of the temperatures. Thus, if at 300 K the hole concentration in the sample B8 was $(6-7) \cdot 10^{18}$ cm$^{-3}$, then at 400 K it increased to $(8-9) \cdot 10^{18}$ cm$^{-3}$. It is also obvious that with increase of the concentration of the majority charge carriers the SCR width is decreased, which is explained from the perspective of the Gauss

theorem, the formula (3). Table 2 shows the measured average MCC concentrations at the room temperature. The measurements were at the low frequency (20−50 kHz), where the frequency dispersion was quite small.

## 2.4. Comparison with the FTIR measurements of the impurity concentration

The spectrum dependences of the transmittance of the samples within the near- and mid-infrared ranges $(700-4000$ cm$^{-1})$ were recorded before deposition of the metal contacts (Fig. 12). The epitaxial CVD-layers were measured using the Nikolet-6700 instrument. The thicknesses of the CVD-epitaxial layers were determined by interference in the IR reflection spectra, which are more sensitive to the optical border between the epitaxial layer and the substrate. The HPHT plates were studied using the Vertex 70 spectrometer with the Hyperion1000 microscope with the resolution 4 cm$^{-1}$ (with averaging along 32 scans).

The FTIR concentration of the partially compensated boron $N_A - N_D$ in the moderately- and heavily-doped samples was evaluated by the experimental spectra using refined empirical calibration dependences of A. Collins in the three bands of the impurity absorption [99], as it is specified in
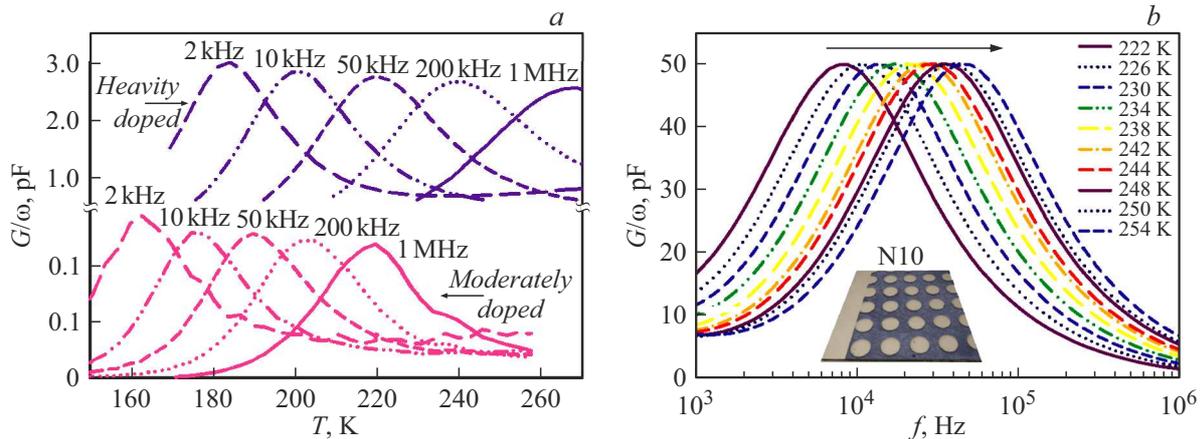
**Figure 13.** *a* — the typical temperature spectra of the conductance of the moderately- and heavily-doped samples; *b* — the frequency spectra of the conductance of the heavily-doped sample N10.

Section 1.2.1:

$$[N_A - N_D](ppm) = 0.0350 \cdot H_{2800},$$

$$[N_A - N_D](ppm) = 0.105 \cdot H_{2458},$$

$$[N_A - N_D](ppm) = 1.00 \cdot H_{1290}, \quad (15)$$

where $H_{2800}, H_{2458}, H_{1290}$ — the amplitude of the corresponding peak in the absorption spectrum. Moreover, for the boron-doped diamond 1 ppm of the impurity is approximately corresponds to its concentration $[N_A - N_D] = 1.67 \cdot 10^{17} \, cm^{-3}$.

The FTIR concentrations of the partially compensated boron impurity, which are obtained from the spectra, are also shown in Table 2.

From the comparison in the table, it can be concluded that the closest results of the $C-V$ and FTIR measurements are observed for the moderately-doped natural samples, in which there is uniform distribution of the boron impurity. This result is expected. The good correlation between the $C-V$ recorded at the reduced frequency of the test signal and the FTIR measurements in the moderately-doped diamond samples was already claimed in the Glover's work in 1973 [106] and was used to be confirmed later. No such close correlation is observed for the CVD-epitaxial layers. It can be explained by a small relative thickness of the boron-doped layer in the total thickness of transmission through the sample by the probing radiation. On the other hand, the capacitance-voltage measurements of the CVD layers require the planar geometry of the contacts due to the undoped substrate, thereby imparting the systematic error to the results of the measurements of the MCC concentration, too.

As the calibration (15) was carried out in relation to the Hall measurements, here we mention the article [90], which demonstrates the substantial difference in the results of the Hall measurements on the uniform samples and on those consisting of several growth sectors. Therefor, the

authors have concluded that the true parameters of the semiconductor diamond could be obtained via the Hall method only provided that the (single-sector) samples are correctly cut out.

Thus, in spite of the wide application of the optical methods (first of all, for jewellery manufacturing), the fundamentally integral measurement result and the required standard calibration (as per the Hall measurements) reduce their electronic grade importance for modern careful and precision characterization of the impurity concentration and do not ensure obtaining the spatial distribution of the impurity within the semiconductor single-crystal diamond.

## 2.5. Activation (ionization) energy of the boron impurity, as determined by the dynamic spectra of the conductance

We have carried out a cycle of the sample measurements using the two methods of the admittance spectroscopy: by scanning on temperature and by scanning on frequency of the measurement signal. We note that the change of the sample temperature within the range $100-400 \, K$ results in the change of the pace of emission of the charge carriers from the deep level in more than $10^{10}$ times as per (10); at the same time the range of the available frequencies of the RLC measuring device is just only 4 orders. Therefore, the temperature spectra should be considered as priority ones. Although, their measurements require additional time and it is quite difficult to technically implement them. Their results can be used to fix a convenient temperature interval and to consequently carry out the precise evolvement of the admittance spectrum as per the frequency at the constant temperature. In regard of the above-said, the authors [128,129], etc. have limited to the scanning by the frequency when measuring the admittance.

The typical spectra of the conductance of the weakly- (IL5, the transparent region) and heavily- (IL5, the blue region) doped samples are shown on Fig. 13. They occupy

**Table 3.** Activation energies and capture sections in the boron-doped samples of the single-crystal diamond, as recorded in the work

| Sample | | Apollo Blue | D11 | B7 | N10 | B11 | IL5, the multi-sector plate, the sector | | | IL9, the multi-sector plate, the sector | | |
|---|---|---|---|---|---|---|---|---|---|---|---|---|
| | | | | | | | T | L | B | T | L | B |
| Origin | | Natural | Natural | CVD | CVD | CVD | HPHT | | | HPHT | | |
| $p$ from $C-V$, $10^{18}$ cm$^{-3}$ (300 K) | | 0.025 | 0.04 | 6.2 | 1.4 | 40 | 0.025 | 0.3 | 2.0 | 0.4 | 3.0 | 12 |
| VB conductance (high $T$) | $E_A$, meV | 322±2 | 320±1 | 250±9 | 230±10 | 101±2 | 326±4 | 315±5 | 274±5 | 323±1 | 328±2 | 166±16 |
| | $A$, $10^4$ ms$^{-1}$·K$^{-2}$ | 25 | 5.3 | 0.11 | 0.019 | 2.9 | 24 | 160 | 1.2 | 230 | 26 | 0.015 |
| | $\sigma$, $10^{-13}$ cm$^2$ | 1.3 | 0.28 | 0.06 | 0.001 | 0.0002 | 1.3 | 8.5 | 0.064 | 35 | 3.9 | 0.002 |
| Hopping conductance | $E_A$, meV | – | – | – | – | 20±4 | – | – | – | – | – | 11±3 |
| $A$, $10^4$ ms$^{-1}$·K$^{-2}$ ($T < 150$ K) | – | – | – | – | 37 | – | – | – | – | – | 90 | |

Note VB — the valence band. The regions are designated as follows: B — blue, L — light blue, T — transparent.

the temperature range of 150−300 K. At the very high degree of doping (the sample B11, IL9, the blue region), the conductance response is also noticeable at the relatively low temperatures due to emergence of a hopping mechanism in the conductance. As per (11), the amplitude of the peaks $G/\omega$ is proportional to the ratio $N_T C_{bar}(T)/p$ and is quantitative data on the concentration of the studied deep center. Thus, within one plate the amplitude of the conductance peaks of the heavily-doped region exceeded the same for the weakly-doped region in more than one order at the same area of the contact Schottky contact (Fig. 13, $a$). This result is fully consistent with the data of the measurements using the MCC $C-V$-concentration method for the multi-sector diamond samples, as shown in Table 2. It should be noted that currently there is almost no publication on the distribution of the boron concentration across the multi-sector diamond plate due to unavailability of relatively large ($> 5 \times 5$ mm) single-crystal plates grown predominantly along the $\langle 111 \rangle$ direction and doped with boron.

The typical spectrum $G-f$ is shown on Fig. 13, $b$ and exemplified by the boron heavily-doped sample N10. Here, the spectrum amplitude is higher than in the blue region of the sample IL5 having the approximately the same impurity concentration, which is due to the larger barrier area and, respectively, the larger capacitance $C_{bar}$. All the samples exhibited the expected shift of the conductance curves with the increase of the frequency into the higher temperatures, which is an integral property of the thermal emission (see Section 1.4.2).

The temperatures of the maximum frequency and temperature spectra of the conductance were taken to plot in the Arrhenius coordinates $\ln(\omega/T^2) = f(1/T)$ using the standard procedure (Fig. 14). The plots were taken to calculate the activation energy $E_A$ of the charge carriers (holes) from the boron impurity level, which corresponds to a certain mechanism of the conductance, as well as the
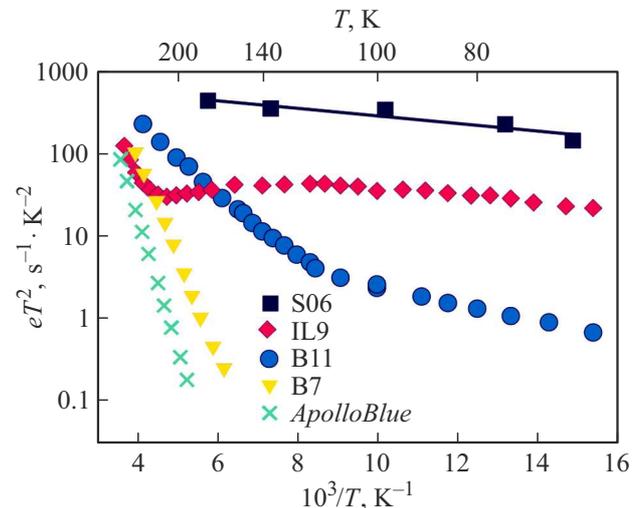


**Figure 14.** Arrhenius plots for the samples with the different boron concentrations.

pre-exponential multiplier $A$ and the hole capture section $\sigma_p$. The obtained activation energies and capture cross sections for the samples are generalized in Table 3. The analysis shows that the thermal activation energy determined from the admittance spectra is always less than the accepted ionization optical energy, which is in principle consistent with the classic considerations [144].

The moderately- and weakly-doped samples are experimentally dotted on the Arrhenius plot and with high accuracy described by a linear dependence across the whole temperature range (Fig. 14). The resultant activation energy is $E_A = 285−325$ meV for the weakly-doped samples, so is $E_A = 215−260$ meV for the moderately-doped ones. The capture section for these samples is $(1−10) \cdot 10^{14}$ and $(1−7) \cdot 10^{15}$ cm$^2$, respectively. In general, in the measurements we have observed the reduction of the
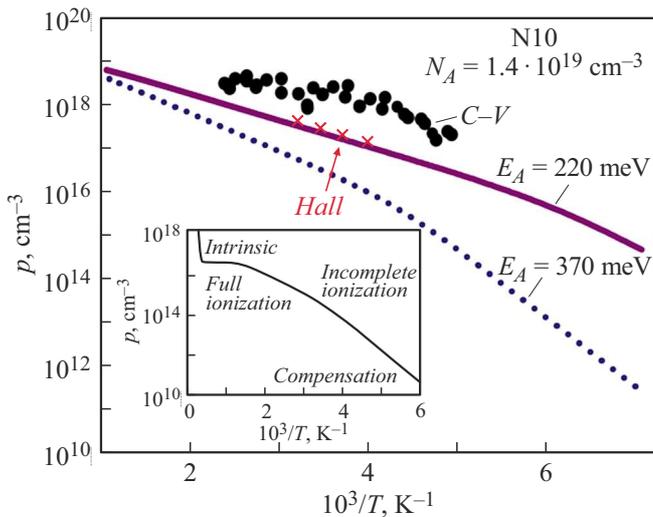
**Figure 15.** Dependence of the hole concentration on the sample temperature N10 (the circles), which is experimentally measured at the low frequency. The solid line is a theoretical calculation of the equilibrium hole concentration for the experimentally-taken $E_A = 220$ meV, the dots — a hypothetical calculation for $E_A = 370$ meV. The crosses designate the expected Hall hole concentration. The insert shows the theoretical equilibrium curve $p_0$ within the wide temperature interval.

activation energy from 325 to 100 meV with increase of the concentration from $2 \cdot 10^{16}$ to $4 \cdot 10^{19}$ cm$^{-3}$. Previously, the work [128] has summarized the table of the boron trap energies in the polycrystalline diamond films measured before 1996 by the various electrical methods. The ionization energies have been recorded to be 0.31 eV (DLTS), 0.36 eV (the charge DLTS, Q-DLTS), 0.29 eV (the photoinduced relaxation current spectroscopy, PICTS), $0.38-0.30$ eV (the temperature dependence of the resistance). The position of the boron level in the thin polycrystalline diamond films had been subsequently measured using the admittance spectroscopy method [145] to provide the activation energy of 0.33 eV. The DLTS measurements of [101,130] for the polycrystalline CVD diamond films (boron moderately-doped ones) have shown a discrete level with the activation energy of $0.35-0.37$ eV. The article [131] has demonstrated that the polycrystalline diamond samples had got the boron activation energy within the interval of $340-360$ meV. It can be seen that the measured energies of the boron activation in the polycrystalline samples are concentrated within the region of $0.29-0.37$ eV, i. e. in the initial part of the „Borst-Lagrange"curve (13). We repeat that the admittance or, in a broader sense, electrophysical measurements of the single-crystal diamond samples are described in the literature much poorly.

The conductance spectra are modelled in accordance with the expression (11), thereby evaluating, in particular, the possible broadening of the impurity band due to the high impurity concentration. As modelled using the respective activation energies and the capture cross sections,

the temperature spectra of the samples exhibited good coincidence with the experimental ones, while the average broadening did not exceed 4 meV. On the contrary, the [145] has observed the strong difference between the experimental and modelled spectra in the admittance method's measurements of the boron impurity in the thin films of the polycrystalline diamond.

The determination of the boron activation energy by the Arrhenius plot included the calculation of a mean square error (MSE) as well, which can also be considered as a crystal perfection criterion. For the natural diamonds, MSE is 1 meV within the entire temperature range, and the synthesized diamond exhibit non-linearity of the Arrhenius plots at the temperatures $\geq 220$ K, which results in the increase of MSE. The recorded non-linearity may be caused by mechanical stresses in the epitaxial layers grown by the CVD method [146] as well as by other electrically active deep centers available in the forbidden band.

We have specified in Section 1.4.4 that the experimental methods of measurement of admittance and impedance, including the $C-V$ method, did not test the thermodynamically equilibrium concentration of the charge carriers, as they require application of the constant and alternating bias to the sample. This fact is not important for the semiconductors with almost full ionization. In such the measurements the wide bandgap diamond exhibits additional ionization of the impurity. Fig. 15 exemplifies the concentrations $p_{CV}$ (the circles) for the sample N10, which are obtained from the $C-V$ experiments within the temperature range of $250-500$ K, and for comparison, the equilibrium MCC concentration $p_0$ on the temperature, as calculated for it. It was calculated by taking the boron activation energy $E_A = 220$ meV determined from AC-conductance spectra of this sample (Fig. 13, $b$). For comparison, there is also a plotted similar dependence with the activation energy of 370 meV. As you can see, in the recorded temperature range the capacitance-voltage measurements demonstrate the substantial (in one order) excess $p_{CV}$ above the expected equilibrium hole concentration in the sample and the same in two orders if it is calculated by a reference energy of boron impurity ionization in the weakly-doped diamond (370 meV). By saturation of the dependence $p = f(\omega, T)$ at the high temperatures we evaluate the impurity concentration in this sample to be $1.4 \cdot 10^{19}$ cm$^{-3}$.

The Hall-method measurements of the concentrations include the application of only a small pulling field and, therefore, it can expect only a small excess of the measured MCC concentration above the thermodynamically equilibrium one (the crosses of Fig. 15).

## 2.6. Hopping conduction for the impurity band

As specified in Section 2.5, we have observed the reduction of the activation energy from 325 to 100 meV with increase of the boron concentration $N_A$ from $2 \cdot 10^{16}$ to $4 \cdot 10^{19}$ cm$^{-3}$. The data on the measurements $E_A$ are summarized in Fig. 16. The obtained results satisfactorily
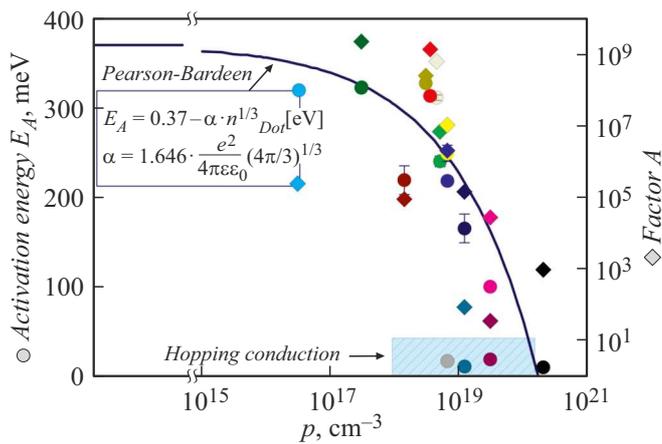
**Figure 16.** Summary plot of the dependence of the activation energy $E_A$ of the boron impurity in diamond and the pre-exponential multiplier $A$ of (10) on the MCC (hole) concentration, as obtained in our measurements. The circles designate the activation energy, so do the small rhombs $A$. The area of the hopping conductivity is dashed in blue.

coincide with the above-said Borst-Lagrange curve (13) for diamond [119,120]. The substantial drop $E_A$ takes place already from $5 \cdot 10^{17}$ cm$^{-3}$. Therefore, the work [19] has incorrectly concluded that it is unnecessary to take into account the change of $E_A$ on $N_A$ in the samples with the concentrations below $10^{18}$ cm$^{-3}$ in order to plot the temperature dependence of the concentration of the free holes $p = f(1/T)$. It should be emphasized that it is this dependence which defines operating properties of the diamond instrument.

In the heavily-doped samples (B11, B9, IL9) we have recorded the replacement of the conductivity mechanism from the common valence band conductivity to the hopping impurity band one. This effect is observed at the temperatures $100-150$ K and above, as it can be seen by transformation of the Arrhenius plot (Fig. 14). In these samples, the activation energy of the thermal-field mechanism of the valence band conductivity is 170 meV with the multiplier $A = 1.5 \cdot 10^5$ s$^{-1} \cdot$ K$^{-2}$ and below, whereas for the hopping impurity band conductivity the activation energy is observed to be just $10-20$ meV. The diamond single crystals with the high boron concentration ($10^{19}-10^{20}$ cm$^{-3}$) were also measured by the authors [147] in the method of the temperature dependence of the resistance. The temperature region above $110-200$ K was observed to have the activation type of conductivity with the activation energy within the range $30-90$ meV. The authors explain the low value of $E_A$ as a result of formation of the conductivity impurity band and the shift of the Fermi level. We note here that the position of the Fermi level is a consequence of the steady processes in the semiconductor crystal, but not a cause thereof.

The necessary conditions of emergence of the hopping conductivity include: the high concentration of the impurity (for emergence of the impurity energy subband), the low

temperature (reducing the direct ejection of the charge carrier into the free band) and the availability of the free states in the impurity band [148]. Usually, the low-temperature hopping mechanism (for example, in Ge with the energy of activation of the impurity $E_A = 13$ meV) we are considering involves presence of some compensation of the material due to the rectangular distribution of the Fermi-Dirac statistics at the cryogenic temperatures. The temperatures above 100 K provide the Fermi-Dirac smooth distribution with availability of the sufficient quantity of the free states.

The hopping conductivity is recorded by us for the diamond samples with the concentrations $N_A \geq 5 \cdot 10^{18}$ cm$^{-3}$, which correlates to the literature data [92,149]. The higher doping degree of the sample, the higher recorded range of the temperatures, at which the hopping mechanism of conductivity prevails. Simultaneously, it is required to increase the frequency for its experimental recording. The ultra-heavily-doped sample S06 ($p_{CV} = 2 \cdot 10^{20}$ cm$^{-3}$) grown by the CVD method already exhibits no evident difference in the observed mechanisms of conductivity, as it can be seen on Fig. 14; its boron activation energy tends to zero ($\leq 11$ meV), which is indicative of the transition to the half-metallic state.

Along with the activation energy, we suggest using the pre-exponential factor $A$, the capture section $\sigma_p$ and the speed of emission of the charge carriers (10) into the respective band in order to separate the different mechanisms of conductivity. In case of the hopping mechanism, the coefficients $A$ calculated from the Arrhenius plot decrease in more than 4 orders, which is determined by the combined reduction of all the multipliers of the expression (10). This effect seems to be attributed to the utmost to the replacement of the effective state density of the valence band $N_V$ to the substantially lower state density of the formed impurity band of boron.

Note that for the semiconductor diamond the high-temperature hopping conductivity can play an importance role in the instrument applications [150,151], radically changing the electrophysical properties of the instrument in the operating mode. It will be more true for the structures of the *n*-type doped by the much deeper impurity of phosphorous.

## Conclusion

The review analyzes the problems and the features of the measurements of the concentration and the activation energy of the boron deep impurity in diamond. A wide interval of the temperatures and the frequencies has been used to perform the careful and precision measurements of the charge carrier concentration in the set of the single-crystal diamond samples of a various nature which are doped with boron of the wide interval of the concentrations. The complex diagnostics of the studied structures has been applied to obtain diverse information about the

morphology, concentration of the impurity and the majority charge carriers. The concentration measurements using the capacitance-voltage characteristics should be considered as the most corresponding to the real operating conditions of the active semiconductor instrument.

It has been shown that the measurements of the concentration of the majority charge carriers in diamond (and in other wide bandgap semiconductors) using the method of the capacitance-voltage characteristics turned out to be substantially non-equilibrium ones. It is due to large energy of ionization of the boron impurity and lagging of the recharging pace of the impurity center behind the change rate (frequency) of the measuring instrument test signal. Thus, in relation to the diamond, the measurements of the barrier capacitance on the voltage should be considered as dynamic [103], but not quasi-static ones. The emerging high variability of the results makes it difficult to routinely interpret the experiment, but at the same time it provides for capabilities of profiling at the various depth of the sample (which are unavailable in the quasi-static mode) and analyzing the frequency-dependent dynamics of formation of the barrier capacitance, thereby extending a pallet of the experimentally-obtained data. In particular, the selection of a region of the temperatures and the frequencies during the measurements enables obtaining specific information about the concentration of both the impurity and the majority charge carriers (holes).

It has been experimentally shown that with increase of the boron concentration in diamond from $2 \cdot 10^{16}$ to $4 \cdot 10^{19}$ cm$^{-3}$ the observed thermal energy of activation of the charge carriers from the acceptor level reduces from 325 to 100 meV. With further increase of the boron concentration, the hopping conductivity of holes for the broadened impurity band takes place, wherein the energy of process activation sharply drops to $10-20$ meV. The speed of the observed thermal-ion emission has been evaluated for the variously-doped samples. It has been found that for the case of the hopping conductivity the pre-exponential multiplier of the emission pace dropped in 4 orders, thereby reflecting the substantial reduction of the mobility of the free holes and the density of the valence band states in comparison with the valence band.

As a result of the performed theoretical and experimental studies as well as analysis of the literature, it has been demonstrated that the admittance spectroscopy including the quasi-equilibrium and non-equilibrium measurement procedures should be considered as one of the most effective non-destructive methods of diagnostics of semiconductor diamond instruments being developed.

## Acknowledgments

## Conflict of interest

The authors declare that they have no conflict of interest.

## References

[1] A. Traoré, P. Muret, A. Fiori, D. Eon, E. Gheeraert, J. Pernot. Appl. Phys. Lett., **104**, 052105 (2014). DOI: 10.1063/1.4864060

[2] P.N. Volpe, P. Muret, J. Pernot, F. Omnés, T. Teraji, Y. Koide, F. Jomard, D. Planson, P. Brosselard, N. Dheilly, B. Vergne, S. Scharnholz. Appl. Phys. Lett., **97**, 223501 (2010). DOI: 10.1063/1.3520140

[3] R. Pilotti, M. Angelone, S. Loreti, G. Pagano, M. Pillon, F. Sarto, M. Marinelli, E. Milani, G. Prestopino, C. Verona, G. Verona-Rinati. Proc. Sci., **240**, 1 (2016). DOI: 10.22323/1.240.0180

[4] A. Metcalfe, G.R. Fern, P.R. Hobson, D.R. Smith, G. Lefeuvre, R. Saenger. J. Instrum., **12**, C01066 (2017). DOI: 10.1088/1748-0221/12/01/C01066

[5] E. Kohn, A. Denisenko. Thin Solid Films, **515**, 4333 (2007). DOI: 10.1016/j.tsf.2006.07.179

[6] M.W. Geis, T.C. Wade, C.H. Wuorio, T.H. Fedynyshyn, B. Duncan, M.E. Plaut, J.O. Varghese, S.M. Warnock, S.A. Vitale, M.A. Hollis. Phys. Status Solidi Appl. Mater. Sci., **215**, 1800681 (2018). DOI: 10.1002/pssa.201800681

[7] S. Koizumi, H. Umezawa, J. Pernot, M. Suzuki (Eds.). *Power Electronics Device Applications of Diamond Semiconductors* (Woodhead Publishing Series in Electronic and Optical Materials, Cambridge, 2018), DOI: 10.1016/C2016-0-03999-2

[8] S.J. Rashid, A. Tajani, L. Coulbeck, M. Brezeanu, A. Garraway, T. Butler, N.L. Rupesinghe, D.J. Twitchen, G.A.J. Amaratunga, F. Udrea, P. Taylor, M. Dixon, J. Isberg. Diam. Relat. Mater., **15**, 317 (2006). DOI: 10.1016/j.diamond.2005.06.019

[9] D.J. Twitchen, A.J. Whitehead, S.E. Coe, J. Isberg, J. Hammersberg, T. Wikström, E. Johansson. IEEE Trans. Electron Devices, **51**, 826 (2004). DOI: 10.1109/TED.2004.826867

[10] J. Achard, F. Silva, R. Issaoui, O. Brinza, A. Tallaire, H. Schneider, K. Isoird, H. Ding, S. Koné, M.A. Pinault, F. Jomard, A. Gicquel. Diam. Relat. Mater., **20** (2), 145 (2011). DOI: 10.1016/j.diamond.2010.11.014

[11] P. Sittimart, S. Ohmagari, T. Yoshitake. Jpn. J. Appl. Phys., **60**, SBBD05 (2021). DOI: 10.35848/1347-4065/abd537

[12] M.P. Dukhnovsky, E.N. Kulikov, A.K. Ratnikova, Yu.Yu. Fedorov, S.A. Bogdanov, A.L. Vikharev, A.M. Gorbachev, A.B. Muchnikov, O.Yu. Kudryashov, K.A. Leont'ev. Elektronnaya tekhnika. Seriya 1 SVCh-tekhnika, **3** (518), 40 (2013) (in Russian).

[13] O. Auciello, S. Pacheco, A.V. Sumant, C. Gudeman, S. Sampath, A. Datta, R.W. Carpick, V.P. Adiga, P. Zurcher, Z. Ma, H.C. Yuan, J.A. Carlisle, B. Kabius, J. Hiller, S. Srinivasan. IEEE Microw. Mag., **8** (6), 61 (2007). DOI: 10.1109/MMM.2007.907816

[14] M. Liao. Funct. Diam., **1**, 29 (2021).
DOI: 10.1080/26941112.2021.1877019

[15] N.I. Alekseev, V.V. Luchinin. *Elektronika almaza* (Izd-vo SPbGETU „LETI", SPb., 2019) (in Russian)

[16] E. Berdermann, M. Pomorski, W. de Boer, M. Ciobanu, S. Dunst, C. Grah, M. Kiš, W. Koenig, W. Lange, W. Lohmann, R. Lovrinčić, P. Moritz, J. Morse, S. Mueller, A. Pucci, M. Schreck, S. Rahman, M. Träger. Diam. Relat. Mater., **19**, 358 (2010). DOI: 10.1016/j.diamond.2009.11.019

[17] S.P. Lansley, H.J. Looi, M.D. Whitfield, R.B. Jackman. Diam. Relat. Mater., **8** (2–5), 946 (1999).
DOI: 10.1016/s0925-9635(98)00423-3

[18] P.J. Sellin, A. Galbiati. Appl. Phys. Lett., **87**, 093502 (2005).
DOI: 10.1063/1.2035885

[19] R.A. Khmel'nitsky, G.V. Chuchueva, N.Kh. Talipov. *Sinteticheskiy almaz dlya elektroniki i optiki* (IKAR, M., 2017) (in Russian)

[20] V.A. Bespalov, V.M. Glazov, E.A. Il'ichev, Y.A. Klimov, S.V. Kuklev, A.E. Kuleshov, R.M. Nabiev, G.N. Petrukhin, B.G. Potapov, G.S. Rychkov, D.S. Sokolov, V.V. Fandeev, E.A. Fetisov, S.S. Yakushov. Tech. Phys., **60**, 553 (2015). DOI: 10.1134/S1063784215040076

[21] G. Chicot, T.N. Tran Thi, A. Fiori, F. Jomard, E. Gheeraert, E. Bustarret, J. Pernot. Appl. Phys. Lett., **101**, 3 (2012).
DOI: 10.1063/1.4758994

[22] H. El-Hajj, A. Denisenko, A. Kaiser, R.S. Balmer, E. Kohn. Diam. Relat. Mater., **17**, 1259 (2008).
DOI: 10.1016/j.diamond.2008.02.015

[23] P.N. Volpe, N. Tranchant, J.C. Arnault, S. Saada, F. Jomard, P. Bergonzo. Phys. Status Solidi — Rapid Res. Lett., **6**, 59 (2012). DOI: 10.1002/pssr.201105480

[24] M. Kunze, A. Vescan, G. Dollinger, A. Bergmaier, E. Kohn. Carbon NY., **37**, 787 (1999).
DOI: 10.1016/S0008-6223(98)00272-3

[25] V.I. Zubkov, M.F. Panov, A.V. Afanas'ev, V.A. Il'in, A.V. Zubkova, I.A. Lamkin, J.E. Butler, A.L. Vikharev, S.A. Bogdanov. Nano- i mikrosistemnaya tekhnika, **12**, 22 (2015) (in Russian).

[26] S. Eaton-Magaña, A. Troy, C.M. Breeding. J. Gems & Gemmol., **26**, 25 (2021).
DOI: 10.15964/j.cnki.027jgg.2021.06.003

[27] V.C. Bormashov, S.A. Tarelkin, S.G. Buga, A.P. Volkov, A.V. Golovanov, M.S. Kuznetsov, N.V. Kornilov, D.V. Teteruk, S.A. Terent'ev, V.D. Blank. Zavodskaya laboratoriya. Diagnostika materialov, **83**, 36 (2017) (in Russian).

[28] V.V. Strelchuk, A.S. Nikolenko, P.M. Lytvyn, S.O. Ivakhnenko, T.V. Kovalenko, I.M. Danylenko, S.V. Malyuta. Semicond. Physics, Quantum Electron. Optoelectron., **24**, 261 (2021).

[29] Y.D. Li, Y.S. Chen, M.J. Su, Q.F. Ran, C.X. Wang, H.A. Ma, C. Fang, L.C. Chen. Chin. Phys. B, **29**, 078101 (2020). DOI: 10.1088/1674-1056/ab90e8

[30] U.F.S. D'Haenens-Johansson, A. Katrusha, K.S. Moe, P. Johnson, W. Wang, Gems & Gemol., **51**, 260 (2015). DOI: 10.5741/GEMS.51.3.260

[31] P.L. Diggle, U.F.S. D'Haenens-Johansson, B.L. Green, C.M. Welbourn, T.N. Tran Thi, A. Katrusha, W. Wang, M.E. Newton. Phys. Rev. Mater., **4**, 093402 (2020). DOI: 10.1103/PhysRevMaterials.4.093402

[32] A. Bogatskiy, J.E. Butler. Diam. Relat. Mater., **53**, 58 (2015). DOI: 10.1016/j.diamond.2014.12.010

[33] A.A. Mayer. *Protsessy rosta kristallov: uch. posobie* (RKhTU im. D.I. Mendeleeva, M., 1999) (in Russian).

[34] A. Paoletti, A. Tucciarone (eds.). *The Physics of Diamond,* in: Proc. Int. Sch. Phys. „Enrico Fermi" (1997), p. 607

[35] J.C. Angus. Diam. Relat. Mater. **49**, 77 (2014).
DOI: 10.1016/j.diamond.2014.08.004

[36] P.M. Martineau, M.P. Gaukroger, K.B. Guy, S.C. Lawson, D.J. Twitchen, I. Friel, J.O. Hansen, G.C. Summerton, T.P.G. Addison, R. Burns. J. Phys.: Condens. Matter, **21**, 364205 (2009). DOI: 10.1088/0953-8984/21/36/364205V.

[37] V. Mortet, A. Soltani. Appl. Phys. Lett., **99** (20), 202105 (2011). DOI: 10.1063/1.3662403

[38] A. Tallaire, J. Achard, F. Silva, O. Brinza, A. Gicquel. Comptes Rendus Phys., **14**, 169 (2013).
DOI: 10.1016/j.crhy.2012.10.008'

[39] A.L. Vikharev, M.A. Lobaev, A.M. Gorbachev, D.B. Radishev, V.A. Isaev, S.A. Bogdanov. Mater. Today Commun., **22**, 100816 (2020). DOI: 10.1016/j.mtcomm.2019.100816

[40] M. Schwander, K. Partes. Diam. Relat. Mater., **20**, 1287 (2011). DOI: 10.1016/j.diamond.2011.08.005.

[41] J.J. Gracio, Q.H. Fan, J.C. Madaleno. J. Phys. D: Appl. Phys., **43** (37), 374017 (2010).
DOI: 10.1088/0022-3727/43/37/374017

[42] B.V. Spitsyn, L.L. Bouilov, B.V. Derjaguin. J. Cryst. Growth., **52** (1), 219 (1981). DOI: 10.1016/0022-0248(81)90197-4

[43] D.I. Sobolev, A.M. Gorbachev, A.L. Vikharev, G.G. Denisov. *Plazmenny reaktor dlya vysokoskorostnogo osazhdeniya almaznykh plenok iz gazovoy phazy* (Patent RF RU 2416677, 2002) (in Russian).

[44] J.E. Butler, Y.A. Mankelevich, A. Cheesman, J. Ma, M.N.R. Ashfold. J. Phys.: Condens. Matter, **21** (36), 364201 (2009). DOI: 10.1088/0953-8984/21/36/364201

[45] A.B. Muchnikov, A.L. Vikharev, A.M. Gorbachev, D.B. Radishev. Diam. Relat. Mater., **20**, 1225 (2011).
DOI: 10.1016/j.diamond.2011.06.030

[46] E.A. Surovegina, E.V. Demidov, M.N. Drozdov, A.V. Murel, O.I. Khrykin, V.I. Shashkin, M.A. Lobaev, A.M. Gorbachev, A.L. Viharev, S.A. Bogdanov, V.A. Isaev, A.B. Muchnikov, V.V. Chernov, D.B. Radishchev, D.E. Batler. Semiconductors, **50**, 1569 (2016). DOI: 10.1134/S1063782616120204

[47] A.Ya. Vul', O.A. Shenderova (red.). *Detonatsyonnye nanoalmazy. Tekhnologiya, struktura, svoistva i primeneniya* (Izd-vo FTI im. A.F. Ioffe, SPb, 2016) (in Russian).

[48] P.P. Sharin, A.V. Sivtseva, V.I. Popov. Tech. Phys., **66**, 275 (2021). DOI: 10.1134/S1063784221020183

[49] A.M. Panich, M. Salti, O. Prager, E. Swissa, Y.V. Kulvelis, E.B. Yudina, A.E. Aleksenskii, S.D. Goren, A.Y. Vul', A.I. Shames. Magn. Reson. Med., **86** (2), 935 (2021).
DOI: 10.1002/mrm.28762

[50] V.A. Plotnikov, S.V. Makarov, D.G. Bogdanov, A.S. Bogdanov. AIP Conf. Proc., **1785**, 040045 (2016).
DOI: 10.1063/1.4967102

[51] K. Hanada. Surf. Eng., **25**, 487 (2009).
DOI: 10.1179/174329409X433939

[52] E. Osawa, D. Ho. J. Med. Allied Sci., **2**, 31 (2012).

[53] J. Barzola-Quiquia, E. Osmic, T. Lühmann, W. Böhlmann, J. Meijer, W. Knolle, B. Abel. Diam. Relat. Mater., **123**, 108891 (2022).

[54] Y. Mindarava, R. Blinder, C. Laube, W. Knolle, B. Abel, C. Jentgens, J. Isoya, J. Scheuer, J. Lang, I. Schwartz, B. Naydenov, F. Jelezko. Carbon, **170**, 182 (2020). DOI: 10.1016/j.carbon.2020.07.077

[55] Y. Mita. Phys. Rev. B — Condens. Matter Mater. Phys., **53**, 11360 (1996). DOI: 10.1103/PhysRevB.53.11360

[56] O.N. Lopatin, A.G. Nikolaev, V.F. Valeev, V.I. Nuzhdin, R.I. Khaibullin. Crystallogr. reports, **63** (3), 327 (2018). DOI: 10.1134/S1063774518030161

[57] V.G. Vins, A.P. Yelisseyev, D.V. Smovzh, S.A. Novopashin, Diam. Relat. Mater., **86**, 79 (2018). DOI: 10.1016/j.diamond.2018.04.022

[58] A.T. Collins, Diam. Relat. Mater., **8**, 1455 (1999). DOI: 10.1016/s0925-9635(99)00013-8

[59] B. Dischler. *Handbook of Spectral Lines in Diamond. Vol. 1: Tables and Interpretations* (Springer-Verlag, Berlin, Heidelberg, 2012), DOI: 10.1007/978-3-642-22215-3

[60] M. Ruf, N.H. Wan, H. Choi, D. Englund, R. Hanson. J. Appl. Phys., **130**, 070901 (2021). DOI: 10.1063/5.0056534

[61] E. Abe, K. Sasaki. J. Appl. Phys., **123**, 161101 (2018). DOI: 10.1063/1.5011231

[62] A.K. Vershovskii, A.K. Dmitriev. Tech. Phys., **65**, 1301 (2020). DOI: 10.1134/S1063784220080216

[63] A.J. Healey, A. Stacey, B.C. Johnson, D.A. Broadway, T. Teraji, D.A. Simpson, J.P. Tetienne, L.C.L. Hollenberg. Phys. Rev. Mater., **4**, 104605 (2020). DOI: 10.1103/PhysRevMaterials.4.104605

[64] D.B. Radishev, M.A. Lobaev, S.A. Bogdanov, A.M. Gorbachev, A.L. Vikharev, M.N. Drozdov. J. Lumin., **239**, 118404 (2021). DOI: 10.1016/j.jlumin.2021.118404

[65] S. Pezzagna, J. Meijer. Appl. Phys. Rev., **8** (2021). DOI: 10.1063/5.0007444

[66] A.I. Zeleneev, S.V. Bolshedvorskii, L.A. Zhulikov, V.V. Sochenko, O.R. Rubinas, V.N. Sorokin, A.N. Smolyaninov, A.V. Akimov. AIP Conf. Proc., **2241**, 020039 (2020). DOI: 10.1063/5.0012326

[67] C. Wang, C. Kurtsiefer, H. Weinfurter, B. Burchard. J. Phys. B At. Mol. Opt. Phys., **39**, 37 (2006). DOI: 10.1088/0953-4075/39/1/005

[68] T. Lühmann, R. John, R. Wunderlich, J. Meijer, S. Pezzagna. Nat. Commun., **10**, 4956 (2019). DOI: 10.1038/s41467-019-12556-0

[69] A. Pershin, G. Barcza, Ö. Legeza, A. Gali. Npj Quantum Inf., **7**, 99 (2021). DOI: 10.1038/s41534-021-00439-6

[70] R. Fukuta, Y. Murakami, H. Ohfuji, T. Shinmei, T. Irifune, F. Ishikawa. Jpn. J. Appl. Phys., **60** (3), 035501 (2021). DOI: 10.35848/1347-4065/abdc31

[71] A.A. Razgulov, S.G. Lyapin, A.P. Novikov, E.A. Ekimov. Diam. Relat. Mater., **116**, 108379 (2021). DOI: 10.1016/j.diamond.2021.108379

[72] V.A. Kukushkin. Tech. Phys., **64** (2), 226 (2019). DOI: 10.1134/S1063784219020105

[73] S.J. Charles, J.W. Steeds, D.J.F. Evans, J.E. Butler. Mater. Lett., **57**, 3690 (2003). DOI: 10.1016/S0167-577X(03)00152-6

[74] J. Barjon, E. Chikoidze, F. Jomard, Y. Dumont, M.A. Pinault-Thaury, R. Issaoui, O. Brinza, J. Achard, F. Silva. Phys. Status Solidi a — Appl. Mater. Sci., **209**, 1750 (2012). DOI: 10.1002/pssa.201200136

[75] S.A. Manifold, G. Klemencic, E.L.H. Thomas, S. Mandal, H. Bland, S.R. Giblin, O.A. Williams. Carbon, **179**, 13 (2021). DOI: 10.1016/j.carbon.2021.02.079

[76] N. Lambert, A. Taylor, P. Hubík, J. Bulíř, J. More-Chevalier, H. Karaca, C. Fleury, J. Voves, Z. Šobáň, D. Pogany, V. Mortet. Diam. Relat. Mater., **109**, 108003 (2020). DOI: 10.1016/j.diamond.2020.108003

[77] A.V. Krasil'nikov, N.B. Rodionov, A.P. Bol'shakov, V.G. Ral'chenko, S.K. Vartapetov, Yu.E. Sizov, S.A. Meschaninov, A.G. Trapeznikov, V.P. Rodionova, V.N. Amosov, A.N. Khmel'nitsky, R.A. Kirichenko. ZhTF, **92**, 596 (2022) (in Russian). DOI: 10.21883/JTF.2022.04.52247.226-21

[78] Yu.V. Gulyaev, A.Yu. Mityagin, V.S. Feschenko, G.V. Chucheva. DAN, **450** (4), 401 (2013) (in Russian).

[79] H. Kawarada, Y. Araki, T. Sakai, T. Ogawa, H. Umezawa. Phys. Status Solidi (A), **185**, 79 (2001). DOI: 10.1002/1521-396X(200105)185:1¡79::AID-PSSA79¿3.0.CO;2-8

[80] C.E. Nebel, D. Shin, B. Rezek, N. Tokuda, H. Uetsuka, H. Watanabe, J.R. Soc. Interface, **4**, 439 (2007). DOI: 10.1098/rsif.2006.0196

[81] Y.V. Pleskov. Russ. J. Electrochem., **38**, 1275 (2002). DOI: 10.1023/A:1021651920042

[82] F. Gao, C.E. Nebel. ACS Appl. Mater. Interfaces., **8** (28), 18640 (2016). DOI: 10.1021/acsami.6b07024

[83] V. Mortet, A. Taylor, M. Davydova, J. Jiránek, L. Fekete, L. Klimša, D. Šimek, N. Lambert, S. Sedláková, J. Kopeček, P. Hazdra. Diam. Relat. Mater., **122**, 108887 (2022). DOI: 10.1016/j.diamond.2022.108887

[84] V. Zubkov, A. Solomnikova, A. Koliadin, J.E. Butler. Mater. Today Commun., **24**, 100995 (2020). DOI: 10.1016/j.mtcomm.2020.100995

[85] V.I. Zubkov, D.E. Batler. Elektronika i mikroelektronika SVCh, **1**, 68 (2015) (in Russian).

[86] M.A. Lobaev, A.M. Gorbachev, A.L. Vikharev, D.B. Radishev, V.A. Isaev, S.A. Bogdanov, M.N. Drozdov, P.A. Yunin, J.E. Butler. Phys. Status Solidi B, **256** (3), 1800606 (2019). DOI: 10.1002/pssb.201800606

[87] N. Mirsaleh-Kohan, W.D. Robertson, R.N. Compton. Mass Spectrom. Rev., **27**, 237 (2008). DOI: 10.1002/mas.20162

[88] P. Blood, J.W. Orton. *The Electrical Characterization of Semiconductors: Majority Carriers and Electron States* (Academic Press, London, 1992)

[89] D.K. Schroder. *Semiconductor Material and Device Characterization: Third Edition* (John Wiley & Sons, Inc., 2005), DOI: 10.1002/0471749095

[90] V.S. Bormashov, S.A. Tarelkin, S.G. Buga, M.S. Kuznetsov, S.A. Terentiev, A.N. Semenov, V.D. Blank. Diam. Relat. Mater., **35**, 19 (2013). DOI: 10.1016/j.diamond.2013.02.011

[91] E.P. Visser, G.J. Bauhuis, G. Janssen, W. Vollenberg, J.P. van Enckevort, L.J. Giling. J. Phys.: Condens. Matter, **4**, 7365 (1992). DOI: 10.1088/0953-8984/4/36/011

[92] T.H. Borst, O. Weis. Phys. Status Solidi (A), **154**, 423 (1996). DOI: 10.1002/pssa.2211540130.

[93] G.E. Yakovlev, D.S. Frolov, V.I. Zubkov. Zavodskaya laboratoriya. Diagnostika materialov, **87**, 35 (2021) (in Russian). DOI: 10.26896/1028-6861-2021-87-1-35-44

[94] P.N. Brunkov, A.A. Gutkin, M.E. Rudinsky, O.I. Ronghin, A.A. Sitnikova, A.A. Shakhmin, B.Y. Ber, D.Y. Kazantsev, A.Y. Egorov, V.E. Zemlyakov, S.G. Konnikov. Semiconductors, **45**, 811 (2011). DOI: 10.1134/S1063782611060078

[95] B. Sermage, Z. Essa, N. Taleb, M. Quillec, J. Aubin, J.M. Hartmann, M. Veillerot. J. Appl. Phys., **119**, 155703 (2016). DOI: 10.1063/1.4946890

[96] D.S. Frolov, G.E. Yakovlev, V.I. Zubkov. FTP, **53** (2), 281 (2019) (in Russian). DOI: 10.21883/FTP.2019.02.47114.8966

[97] V.F. Lebedev, D.V. Bulyga, A.V. Kolyadin. Pis'ma v ZhTF, **46**, 7 (2020) (in Russian).

[98] P.R. Griffiths, J.A. De Haseth. *Fourier Transform Infrared Spectrometry: 2nd Edition* (Wiley-Blackwell, 2007), DOI: 10.1002/047010631X

[99] D. Howell, A.T. Collins, L.C. Loudin, P.L. Diggle, U.F.S. D'Haenens-Johansson, K.V. Smit, A.N. Katrusha, J.E. Butler, F. Nestola. Diam. Relat. Mater., **96**, 207 (2019). DOI: 10.1016/j.diamond.2019.02.029

[100] J. Walker. Reports Prog. Phys., **42**, 1605 (1979). DOI: 10.1088/0034-4885/42/10/001

[101] V.I. Polyakov, A.I. Rukovishnikov, N.M. Rossukanyi, V.G. Ralchenko. Diam. Relat. Mater., **10**, 593 (2001). DOI: 10.1016/S0925-9635(00)00492-1

[102] L.S. Berman. *Emkostnye metody issledovaniya poluprovodnikov* (Nauka, L., 1972) (in Russian).

[103] V.I. Zubkov. *Diagnostika poluprovodnikovykh nanogeterostruktur metodami spektroskopii admittansa* (Elmor, SPb, 2007) (in Russian).

[104] L.S. Berman, A.A. Lebedev. *Emkostnaya spektroskopiya glubokikh tsentrov v poluprovodnikakh* (Nauka, L., 1981) (in Russian).

[105] A.R. Peaker, V.P. Markevich, J. Coutinho. J. Appl. Phys., **123**, 161559 (2018). DOI: 10.1063/1.5011327

[106] G.H. Glover. Solid State Electron., **16**, 973 (1973). DOI: 10.1016/0038-1101(73)90196-2

[107] D.S. Frolov, V.I. Zubkov. Semicond. Sci. Technol., **31**, 125013 (2016). DOI: 10.1088/0268-1242/31/12/125013

[108] O.V. Konstantinov, O.A. Mezrin. FTP, **17**, 305 (1983) (in Russian).

[109] Yu.A. Gol'dberg, O.V. Ivanova, T.V. L'vova, B.V. Tsarenkov. FTP, **17**, 1068 (1983) (in Russian).

[110] T. Humer-Hager. Semicond. Sci. Technol., **3**, 553 (1988). DOI: 10.1088/0268-1242/3/6/007

[111] V.I. Zubkov. FTP, **40**, 1236 (2006) (in Russian). DOI: 10.1134/S1063782606100149

[112] A.T. Collins, E.C. Lightowlers, *In: The Properties of Diamond,* ed. by J.E. Field (Academic, London, 1979), p. 3.

[113] G.Sh. Gildenblat, P.E. Shmidt. In: *Handbook Series on Semiconductor Parameters: vol. 1.* Ed. by M. Levinshtein, S. Rumyantsev, M. Shur (World Scientific, London, 1996)

[114] V.N. Ovsyuk. *Elektronnye protsessy v poluprovodnkakh s oblastyami prostranstvennogo zaryada* (Nauka, M., 1984) (in Russian).

[115] N.A. Poklonski, S.A. Vyrko, O.N. Poklonskaya, A.I. Kovalev, A.G. Zabrodskii. J. Appl. Phys., **119** (24), 245701 (2016).

[116] V.I. Zubkov, M.A. Melnik, A.V. Solomonov, E.O. Tsvelev, E.O. Bugge, M. Weyers, G. Tränkle, Phys. Rev. B, **70**, 075312 (2004). DOI: 10.1103/PhysRevB.70.075312

[117] C.S. Hung, J.R. Gliessman. Phys. Rev., **96** (1954) 1226. DOI: 10.1103/PhysRev.96.1226

[118] H. Fritzsche. Phys. Rev., **99**, 406 (1955). DOI: 10.1103/PhysRev.99.406

[119] T.H. Borst, O. Weis. Diam. Relat. Mater., **4**, 948 (1995). DOI: 10.1016/0925-9635(94)00263-0

[120] J.-P. Lagrange, A. Deneuville, E. Gheeraert. Diam. Relat. Mater., **7**, 1390 (1998).

[121] D. Blackmore. *Solid body physics* (Mir, M., 1988).

[122] A.V. Los, M.S. Mazzola. Phys. Rev. B, **65**, 165319 (2002). DOI: 10.1103/PhysRevB.65.165319

[123] G. Vincent, D. Bois, P. Pinard. J. Appl. Phys., **46**, 5173 (1975). DOI: 10.1063/1.322194

[124] D.L. Losee. J. Appl. Phys., **46**, 2204 (1975). DOI: 10.1063/1.321865

[125] J. Bardeen, G.L. Pearson. Phys. Rev., **75**, 865 (1949).

[126] J.C. Bourgoin, J. Krynicki, B. Blanchard. Phys. Status Solidi, **52**, 293 (1979). DOI: 10.1002/pssa.2210520132

[127] N.A. Poklonskiy, S.A. Vyrko, A.N. Derevyago. Zhurnal BGU. Fizika, **2** (2), 28 (2020) (in Russian).

[128] S. Nath, J.I.B. Wilson. Diam. Relat. Mater., **5**, 65 (1996). DOI: 10.1016/0925-9635(96)80007-0

[129] Y. Koide, S. Koizumi, H. Kanda, M. Suzuki, H. Yoshida, N. Sakuma, T. Ono, T. Sakai. Diam. Relat. Mater., **14**, 2011 (2005). DOI: 10.1016/j.diamond.2005.08.006

[130] V.I. Polyakov, A.I. Rukovishnikov, B.M. Garin, L.A. Avdeeva, R. Heidinger, V.V. Parshin, V.G. Ralchenko. Diam. Relat. Mater., **14**, 604 (2005). DOI: 10.1016/j.diamond.2004.10.001

[131] A.J. Chiquito, O.M. Berengue, E. Diagonel, J.C. Galzerani, J.R. Moro. J. Appl. Phys., **101** (3), 033714 (2007). DOI: 10.1063/1.2436984

[132] V.I. Zubkov, O.V. Kucherova, S.A. Bogdanov, A.V. Zubkova, J.E. Butler, V.A. Ilyin, A.V. Afanas'ev, A.L. Vikharev. J. Appl. Phys., **118**, 145703 (2015). DOI: 10.1063/1.4932664

[133] V.I. Zubkov, A.V. Solomnikova, J.E. Post, E. Gaillou, J.E. Butler. Diam. Relat. Mater., **72**, 87 (2017). DOI: 10.1016/j.diamond.2017.01.011

[134] A.T. Collins, E.C. Lightowlers. Phys. Rev., **171**, 843 (1968).

[135] F. Capasso, G. Margaritondo (eds.). *Heterojunction Band Discontinuities: Physics and Device Applications* (North-Holland, Amsterdam, 1987)

[136] W.-H. Chang, W.Y. Chen, M.C. Cheng, C.Y. Lai, T.M. Hsu, N.-T. Yeh, J.-I. Chyi. Phys. Rev. B, **64**, 125315 (2001). DOI: 10.1103/PhysRevB.64.125315

[137] V.I. Zubkov, C.M.A. Kapteyn, A.V. Solomonov, D. Bimberg. J. Phys.: Condens. Matter., **17** (15), 2435 (2005). DOI: 10.1088/0953-8984/17/15/014

[138] V.I. Zubkov, I.S. Shulgunova, A.V. Solomonov, M. Geller, A. Marent, D. Bimberg, A.E. Zhukov, E.S. Semenova, V.M. Ustinov. Izvestiya RAN. Seriya fizicheskaya, **71** (111), 2007 (in Russian).

[139] V.I. Zubkov, I.V. Ivanova, M. Weyers. Appl. Phys. Lett., **119**, 043503 (2021). DOI: 10.1063/5.0056842

[140] S. Zi. Physics of Semiconductor Devices (Mir, M., 1984).

[141] O.V. Kucherova, V.I. Zubkov, E.O. Tsvelev, I.N. Yakovlev, A.V. Solomonov. Zavodskaya laboratoriya. Diagnostika materialov, **76** (3), 24 (2010) (in Russian).

[142] V.I. Zubkov, O.V. Kucherova, I.N. Yakovlev, A.V. Solomonov. Mikroelektronika, **44**, 234 (2015) (in Russian).

[143] E. Gaillou, J.E. Post, D. Rost, J.E. Butler. Am. Mineral., **97**, 1 (2012). DOI: 10.2138/am.2012.3925

[144] S.M. Ryvkin. *Fotoelektricheskiye yavleniya v poluprovodnikakh* (Fizmatgiz, M., 1963) (in Russian).

[145] J.W. Glesener, K.A. Snail, A.A. Morrish. Appl. Phys. Lett., **62**, 181 (1993).

[146] H. Pinto, R. Jones, J.P. Goss, P.R. Briddon. J. Phys.: Conf. Ser., **281** (1), 012023 (2011). DOI: 10.1088/1742-6596/281/1/012023

[147] G.A. Buga, S.G. Blank, V.D. Terent'ev, S.A. Kuznetsov, M.S. Nosukhin, S.A. Kul'bachinskiy, V.A. Krechetov, A.V. Kytin, V.G. Kytin. ZhETF, **131**, 662 (2007) (in Russian).

[148] V.I. Fistul'. *Sil'nolegirovannye provodniki* (Nauka, M., 1967) (in Russian).

[149] K. Thonke. Semicond. Sci. Technol., **18**, S20 (2003). DOI: 10.1088/0268-1242/18/3/303

[150] T. Inushima, T. Matsushita, S. Ohya, H. Shiomi. Diam. Relat. Mater., **9** (3), 1066 (2000). DOI: 10.1016/S0925-9635(00)00226-0

[151] K. Oyama, S.-G. Ri, H. Kato, M. Ogura, T. Makino, D. Takeuchi, N. Tokuda, H. Okushi, S. Yamasaki. Appl. Phys. Lett., **94**, 152109 (2009). DOI: 10.1063/1.3120560